UNIVERSITEIT VAN AMSTERDAM

Universiteit Utrecht

An analysis of XMM-Newton data of M31

L.C. Oostrum
June 2013

Supervisors:
Dr. M.J. Middleton (UvA)
Prof. Dr. H.C. Gerritsen (UU)

Abstract

Two observations by X-Ray satellite XMM-Newton of the Andromeda galaxy have been examined. Relevant radiative processes are explained. Extracting information from sources is done using the XMM-Newton software. Both light curves and spectra are made. These are the main tools for identification. Furthermore, variability, hardness ratios and luminosities are calculated. These help classify a source. Twelve bright sources are classified. Three sources are more interesting and are investigated further. These include the first microquasar ever found outside our galaxy, a super soft source and a Z source candidate, of which only nine are known.

Contents

1 Introduction

This project is about the identification of X-Ray sources in M31, the Andromeda galaxy. These source can be X-Ray binaries (XRB), supernova remnants (SNR) or possibly sources not really in Andromeda such as active galactic nuclei (AGN) or globular clusters (GLC). M31 is one of the most studied objects in the sky. It is the nearest large galaxy, at a distance of about 0.78 Mpc. Due to its size and low distance, it has an angular diameter of over 3 degrees in the sky. This makes it possible to identify individual sources in the galaxy. There is not much absorption between us and M31, making it easier to take a good look at the stars in the galaxy. M31 seems to be very similar to our own galaxy, although it is a bit bigger. Therefore the source population in M31 could tell us something about the source population in our galaxy. It is very hard to get the full picture of our own galaxy as a large part is obscured by gas and dust. Understanding the source population in galaxies is important because it can help us understand the structure of galaxies and the evolution of both galaxies and stars. If one wants to get real physical information about a source, the identification of that source has to be accurate. This is not always easy, as different types of sources can look very similar. The brightest sources in the field are to be identified. The most interesting ones will be investigated further.

2 Theory

2.1 Radiative processes in XRBs

XRBs consist of a white dwarf (WD), neutron star (NS) or black hole (BH) with a companion star. The companion star often loses mass to the compact star in a process known as Roche lobe overflow. The Roche lobe is the maximum volume of a certain object in a binary system. Figure 1 shows equipotential lines. Along these lines, matter is equally strong bound to the objects.

There are some places where the potential is zero.

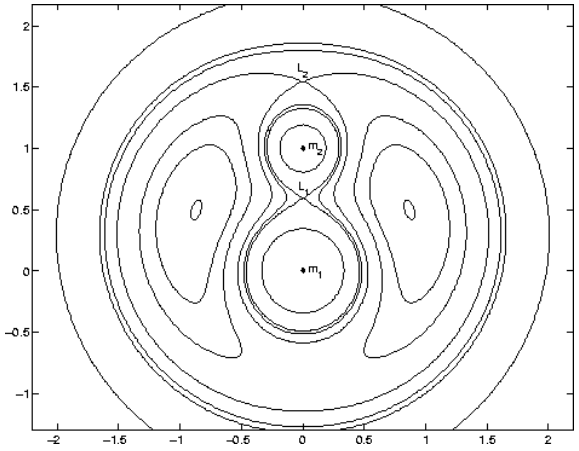

Figure 1: *Equipotential lines. The lower star is the heavier one. The L_1 point between the two stars is very important as here the potential is zero and matter can flow from one star to the other.*

These are the Lagrange points. The most important one is L_1. This point lies between the two objects, closer to the heavier one. When the radius of the companion star equals the distance between the center of that star and the L_1 point, it can start to lose matter through this point to the other star. The volume of the companion star at this point is the Roche lobe volume. Matter that is lost to the other star can form a disk. This is known as an accretion disk. The matter in this disk flows inwards, eventually ending up on the surface of the compact star (or in the case of a black hole, beyond the event horizon). The infalling matter releases energy. This has a black body spectrum, as described in equation 1. Here ν is the photon frequency and T is the disk temperature. The photon frequency is related to its energy by $E = h\nu$.

$$I = \frac{2h\nu^3}{c^2} \frac{1}{e^{\frac{h\nu}{kT}} - 1} \tag{1}$$

As different parts of the disk have different temperatures, a multi-temperature black body is observed, often called disk black body. The black body spectrum can be altered by thermal comptonization. This broadens the black body. Comptonization is

the alteration of photon energy through interaction with matter. In practice, this means that the high energy end of the black body is comptonized and moves further to the right. Comptonization is described by equation 2 (Done 2010 [6]).

$$E_{out} = \frac{E_{in}(1 - \beta \cos\theta_{ei})}{1 - \beta \cos\theta_{e0} + (E_{in}/\gamma)(1 - \cos\theta_{io})} \quad (2)$$

A disk black body is mostly observed in black hole binaries (BHBs) with a high accretion rate. If the accretion rate is high, a lot of energy is released every second. This results in a bright disk. This is called the thermal or soft state of a BHB.

In low rate BHBs, a power law is seen. A power law is radiation of the type given in 3. Here E is the photon energy, N_0 is the intensity of photons at 1 keV and Γ is the so-called photon index. The units of $N(E)$ are photons per second per centimeter squared per energy band. The flux is then equal to $EN(E)$. The energy per bin is $F(E)dE = F(E)EdE/E = EF(E)d\log E$. So plotting $EF(E)(= E^2N(E))$ versus $\log(E)$ shows at which energy the source luminosity peaks (Done 2010 [6]).

$$N(E) = N_0 E^{-\Gamma} \quad (3)$$

The disk is weak compared to the power law in low rate BHBs, so just a power law spectrum is seen. Sometimes a weak black body can still be observed at low energies. This is called the hard state. A BHB can switch between low and high accretion rates, so the spectrum changes over time.

The BHB section also applies to neutron stars (NS). The main difference between the two is that NS have a surface, whereas BHBs have an event horizon. There can be outbursts on a NS surface, but this usually will not be seen in the spectrum. It can be seen in the light curve, as explained in section 2.2. It is therefore hard to distinguish between NS and BHBs by just their spectrum.

Power laws can also be observed in many other objects, like active galactic nuclei (AGN) or globular clusters (GLC). AGN are much farther away than M31, but that is often impossible to measure. If a power law is the only feature measured, it may be hard to classify the source. A solution is to look up the optical counterpart in a catalog. These can be the companion stars of the X-Ray source. This is only true if the optical emission of the X-Ray source, due to e.g. an accretion disk, is very low. If the optical counterpart is an high-mass star like an O or B star, the source is a high mass X-Ray binary (HMXB). If the optical counterpart is a low mass star like a K or M star, it is a low mass X-Ray binary (LMXB).

The last type of radiation that is probably observed is Bremsstrahlung. Bremsstrahlung literally means braking radiation. This occurs when charged particles are decelerated by interaction with other particles. Mostly the particle is an electron deflected by an atomic nucleus. The particle then produces electromagnetic radiation. This can happen for example in cooling shocked plasma (which e.g. appears in supernova remnants (SNR)) or accreting cataclysmic variables (CVs). CVs are white dwarfs that suddenly increase in brightness. After a short time, they decrease again to their original brightness. These outbursts are caused by an instability in the white dwarfs accretion disk, causing material from the disk to fall onto the surface of the star. The temperature rises enough to start nuclear fusion. All material is then fused, resulting in a very sudden but short increase in brightness. There are several subclasses of CVs, as the way the increase in brightness happens can vary. Two main classes are novae [14] and polars [4].

All types of radiation are influenced by absorption. There is a small amount of mostly neutral hydrogen, but also some other elements such as helium and oxygen, between M31 and us. This gas absorbs certain energy photons. The absorption is measured as the amount of atoms in a column of one square meter between the source and us (n_H). For M31 the hydrogen absorption is about $7 * 10^{20}$. This was calculated using a tool on the HEASARC web page,

which can be found at http://heasarc.gsfc.nasa.gov/. I used the absorption as measured by Dickey and Lockman, 1990 [5].

2.2 XRB variability

The brightness of XRBs can change over time. This can help identify a source, but is only possible if the quality of the data is good enough, so the variability is significant. GLC and SNR are usually not very variable. Strong variability thus suggests a source is a XRB.

Variability is also important when distinguishing between NS and BHBs. Both have similar spectra, as discussed in section 2.1. Some processes are only possible if an object has a surface. A BHB does not have a surface, so if such a process is seen, the object cannot be a BHB. Two processes are discussed here.

The first is X-Ray pulsation. This can occur when the NS has a very strong magnetic field ($> 10^{12}$ G). The accretion near the star is then influenced by the magnetic field. The infalling matter follows the magnetic field and ends up on the surface of the star at the magnetic poles. There a lot of radiation is produced. We can see this radiation only if one of the magnetic poles faces us. If the magnetic poles do no coincide with the axis of rotation, the brightness of the star will vary. Sometimes we will not see the magnetic pole, so no radiation from the infalling matter is observed. Sometimes the pole does face us and we will see more radiation. This variability shows a rise and fall in brightness, with a period equal to either the rotation period of the star if we see only one magnetic pole, or half the period if we see both poles.

The other process is a X-Ray outburst, also known as type-I burst. This is similar to outbursts in a CV. Matter that falls onto the surface of the NS causes a thermonuclear explosion. This increases the brightness a lot, but for a very short time.

SNR and CVs can also look very similar, both can have a bremsstrahlung spectrum. SNR are mostly constant, whereas CVs could have more variability.

Variability on a very short timescale can thus indicate either a NS with type-I outbursts or a CV. Variability on a longer timescale can help distinguish between NS and BHBs. Most sources will not show any variability at all, or the data quality may too poor to detect variability. Then the identification fully relies on spectral analysis.

3 Methods

3.1 XMM-Newton

XMM-Newton is a X-Ray satellite made by ESA. It is equipped with some of the most sensitive CCD chips ever made. The data used for this thesis came from the EPIC pn detector. This detector consists of twelve identical CCDs. Each one of them has a resolution of 384x400 pixels. The chips can be read out very fast, more than a thousand times per second. This allows detection of very fast variability. I have used a time resolution of 10 or more seconds, since the data quality was not good enough to do better. The detector is most sensitive to photons with energies in the range 3-10 keV. This makes it a good detector for XRBs. My data consists of two observations of M31 made by the EPIC pn detector, both of the same region near the center of the galaxy. These observations are about 30 arcminutes across. They contain numerous sources.

3.2 Soft proton flaring

Soft protons can affect the observations. These protons seem to exist in clouds in the Earth's magnetosphere, as described in the XMM-Newton User Handbook section 3.3.7 [9]. If XMM-Newton moves through such a cloud during an observation, the protons will be detected. This results in a very high background rate in the observation, called flaring. Figure 2 shows an observation badly affected by soft proton flaring. The flaring occurs around 10-15 keV. Therefore a light curve of the 10-15 keV band is produced for each observation. This is used to check if the observation is affected by flaring. It is also

used to determine when the flaring occurs, so these times can be removed from the data.

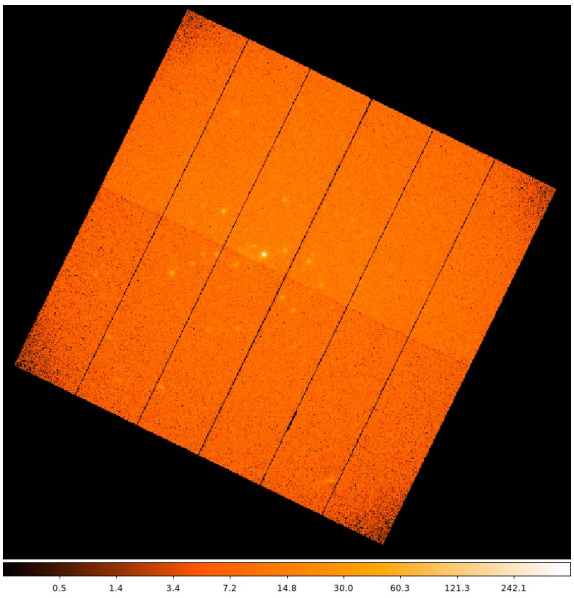

Figure 2: *Observation badly affected by soft proton flaring. The edges of the twelve CCDs can still be seen.*

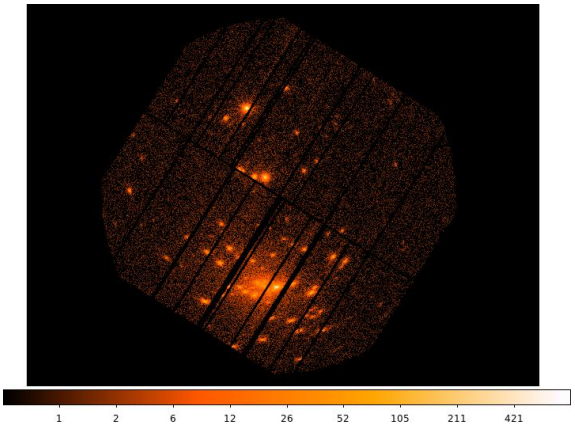

Figure 3: *Full field of the first observation. The black lines are locations with bad pixels and/or the edges of the CCDs. Most sources are in the bottom half of the field.*

3.3 Extracting data

For the analysis both spectra and light curves of individual sources are needed. The first observation was made on July 28, 2012, with an exposure of 10 ks (observation ID 0700380501). The second observation was made about a week later on August 8, 2012, with an exposure of 25 ks (observation ID 0700380601). I started with analyzing only the first observation. An image is extracted from the data as shown in figure 3. This image is already corrected for bad pixels and CCD edges.

The XMM-Newton software (SAS) contains xmmselect, a package for extracting sources from a dataset and calculating their spectra and light curves. It uses a selection expression, which determines how the data is processed. I used FLAG==0 and PATTERN<=4. FLAG determines what is to be done with the bad pixels. FLAG==0 means that bad pixels are ignored (they are put to zero counts) and pixels next to a bad pixel are also ignored. This is important because one photon can be spread over multiple pixels. This is due to the fact that photons are not detected directly. They produce electrons, which are detected. These electrons don't necessarily end up in the same pixel. If a photon is spread over multiple pixels, the energy of the photon has to be calculated from multiple events and will be more uncertain. PATTERN<=4 makes sure only photons which are singles or doubles (in one pixel or spread over two) are taken into account.

Before proceeding to the extraction of individual sources, soft proton flaring has to be removed. This is done by making a light curve of the high energy band (10-15 keV). If the observation is affected by flaring, the count rate will be very high in comparison to the normal rate. By looking at the light curve, the normal rate is determined. Then a file with the good time intervals (GTI) in it is made using tabgtigen which either removes everything above a certain rate, or specified time intervals. A link to the GTI file is then added to the selection expression in xmmselect.

Analysis is done using both spectral and timing

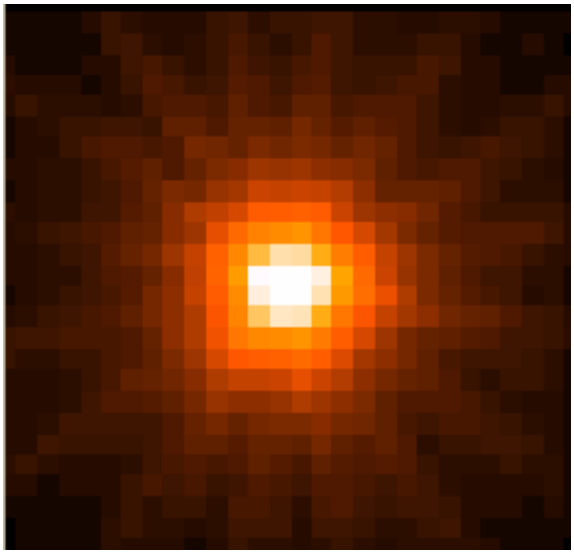

Figure 4: The PSF of the XMM-Newton telescope seen by the pn detector [10].

methods. Therefore light curves and spectra are extracted for individual sources. This is done in a few steps.

First, a source region has to be selected. This was done using DS9 an imaging program, which shows the image of the observation in real sky coordinates, instead of just an arbitrary x and y axis. This makes it possible to select a region in the image, which will be the same region in the sky when loaded into any other image. Sources do not appear as dots on the image, but they are spread out. This is due to the detector. The point spread function (PSF) describes how a point source is spread out. Maybe one of the most famous examples of the influence of the PSF is the fact that bars often appear in images of stars. This happens because the secondary mirror in a telescope is held in place by a few bars. See figure 4.

The pn detector spreads out point sources with a full width at half maximum (FWHM) of about 6.6 arcseconds. This means that 6.6 arcseconds away from the center of a source, the intensity of the source is half of the intensity in the center of the source. It is clear that a circular region around a source has to be selected to get all data from a single source. It is impossible to get all photons from a source, as there are other sources in the field and light from those sources is unwanted. The source region has to be selected carefully. If it is too small, there is not enough data in it. If it is too large, there might be other sources interfering. For the pn detector, 42 arcseconds is known to be a good size for the source region. About 90% of the source flux is contained in a region that size as described in the XMM-Newton User Handbook section 3.2.1.1 [10]. Most of the time however, sources are so close to each other that a smaller region has to be used. In a region 20 arcseconds in size, 80% of the flux is contained [10]. The pn detector has an angular resolution of about 3 arcseconds, so sources closer to each other than that cannot be distinguished. This also means the position of a source has an uncertainty of about 3 arcseconds.

Ideally, the source region only has photons from the actual source in it. However, there is always an amount of background noise. This noise has to be subtracted from the source data. So secondly, a background region has to be selected. Every CCD has a different noise profile, so it has to be on the same chip as the source region, if possible. CCDs never read out their data perfectly, a source gets spread out in the readout direction. The background region cannot contain another source and should not be in the readout direction seen from any source. That way the background really contains only background noise. After selecting these regions, a light curve is made of both using xmmselect. These curves are binned to 10 s. This means every data point contains the data of 10 s of the observation. Since it's a 10 ks observation, this results in 1000 bins. The background light curve is subtracted from the source light curve, to get a curve with only actual source data in it. This is done by using lcmath, part of the HEASOFT software. To get reliable data, only sources with over 1000 counts were used. This makes sure there are enough data points for spectral fitting. When there are too little data points, almost

any fit will be a good fit so nothing can really be concluded.

Thirdly, spectra are made. This is also done using xmmselect. Four files are produced: the source spectrum, the background spectrum and two response files (RMF and ARF). The spectra are grouped to contain at least 25 photons in each bin. This is to make sure the distribution is Gaussian, so Gaussian statistics can be used. All spectral information is stored in one file, which points to the other spectral files. The response files describe how the detector responds to a photon with a certain energy. A photon with e.g. an energy of 3 keV is not necessarily detected as 3 keV. It may well be detected as 3.1 keV, or even 4 keV. The response matrix file (RMF) describes the chance a photon with energy E is detected as having another energy $E + \Delta E$. The detector has a limited energy resolution, $E/\Delta E \sim 20$ to 50 in case of the pn detector, so the response function is not continuous. That is why it results in a matrix file. The auxiliary response file (ARF) contains information about the effective area and quantum efficiency of the detector. The source spectrum multiplied by both the RMF and ARF produces the spectrum as it is observed by the detector.

Together with instrument calibration files provided by ESA, the light curves and spectra are the files used for further analysis.

When the first observation has been processed, the above procedure is repeated for the second one.

3.4 Other quantities

In addition to the light curves and spectra, a few more calculations will be made for each source. The light curves are mostly used to detect possible variability of a source. To quantize the variability, the fractional variability is calculated as defined in equation 4. Here S is the total variance of the light curve, $< \sigma_{err}^2 >$ is the mean error squared, $< X >$ is the mean count rate, all defined in the usual way (Edelson et al. 2002 [8]).

$$F_{var} = \frac{1}{< X >} \sqrt{S^2 - < \sigma_{err}^2 >} \tag{4}$$

In addition to this, a power density spectrum (PDS) is calculated. This is the fouriertransform of the light curve as given by equation 5. Here $N(t)$ is the count rate as function of time, which is the light curve. $P(\nu)$ is the power as function of frequency, which is the PDS.

$$P(\nu) = \frac{1}{\sqrt{2\pi}} \int N(t) e^{i\nu t} dt \tag{5}$$

If there is a strong variability with a frequency of .1 Hz, the amplitude of that frequency will be high compared to the others. The amount of variability detectable with the PDS depends on the time binning. A time binning of 10s is used. The fastest variability that can be observed is then the nyquist frequency, .05 Hz. This is half the frequency corresponding to binning of 10s. It is not .1 Hz because information about the .05 - .1 Hz band can still be interpolated from the data. The segment are rebinned using a geometric series with step .25. This makes sure the bins are more or less equally wide in log space. It also means higher frequency bins contain more data points. Therefore the uncertainties are lower in those bins than in the bins with a lower frequency. See figure 5 for an example. This PDS shows some variability, at frequencies below 1E-03 Hz, however these bins have fairly large uncertainties.

As an easy and quick method of identification, the hardness ratio of each source is calculated. Essentially, the hardness ratio (HR) is a measure of the colour of the source, although it is not a visible colour since we are looking at X-Rays. The HR is defined as the difference between the 'hard' (high energy) and 'soft' (low energy) flux, divided by the total flux. I chose .3-3 keV as low energy band and 3-10 keV as high energy band. This gives a HR as given in equation 6. The HR varies between minus one and one. It is one if the soft flux is zero and minus one if the hard flux is zero. It is zero when both are equal.

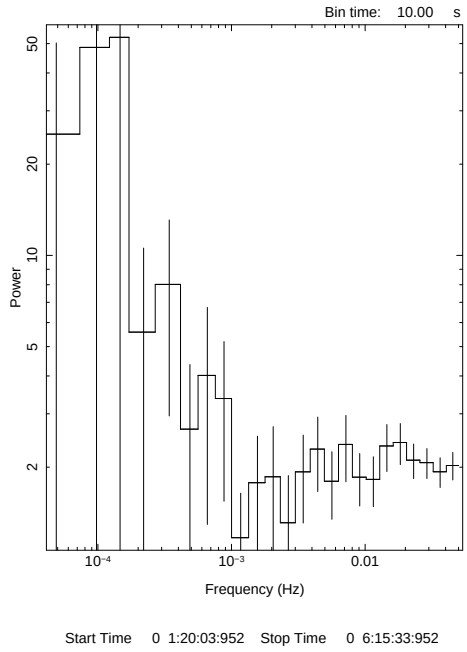

Figure 5: *PDS example. There is some variability below 1E-03 Hz, but these bins have large uncertainties.*

$$HR = \frac{F_{3-10} - F_{.3-3}}{F_{3-10} + F_{.3-3}} \tag{6}$$

To help distinguish BHB and NS, the luminosity can be calculated. Luminosity is simply the power of the source. The Eddington limit poses a theoretical maximum for the luminosity due to accretion. It only applies to a fully ionized hydrogen gas and spherically symmetric accretion. This usually does not apply, as most accretion happens in a disk. Observations do imply the Eddington limit is an important limit, as there are no known sources with an accretion luminosity much higher than the Eddington limit. The limit assumes the infalling matter is pulled towards the star by gravity and pushed away by radiation pressure. If an electron is pushed away, it takes a proton with it through the Coulomb force. Equaling the force due to gravity (left hand side of equation 7) and the force due to radiation (right hand side of equation 7) gives the Eddington luminosity (equation 8. Here M is the mass of the star, m_p is the mass of a proton, σ_t is the Thompson cross section and r is the distance to the star.

$$\frac{GMm_p}{r^2} = \frac{\sigma_t L_{edd}}{r\pi r^2 c} \tag{7}$$

$$L_{edd} = \frac{4\pi GMm_p c}{\sigma_t} = 1.26E38\, M/M_\odot\, ergs/s \tag{8}$$

The luminosity can be calculated from the flux with $L = 4\pi r^2 F$. Here r is the distance to the object. The distance to M31 is assumed to be 788 kpc. The maximum mass of a NS is not exactly known, but is estimated to be around $2M_\odot$. This gives an Eddington limit of about 2.5E38 ergs/s. A source much brighter than this will probably be a BHB.

3.5 Source identification

Two types of analysis were done to identify a source. A timing analysis using the light curve, PDS and F_{var}, and a spectral analysis using the spectrum and HR. The spectra are fitted using XSpec. This is a spectral fitting package in the XMM-Newton software (SAS). It can display a spectrum and has a wide range of models available for spectral fitting. The fits generate a list of parameters with their errors, as well as χ^2 statistical quantities. It can also compute the flux in a certain energy band.

The spectral data is loaded into XSpec. Then a power law with $N_0 = 1$ and Γ=0 is applied. $E^2N(E)$ is plotted versus $\log(E)$. The model is then a flat line, so only the data is shown. This has to be done this way because XSpec cannot show the source data in $E^2N(E)$ space without a model. Then a model to be fitted is selected by eye.

The model names in XSpec are tbabs for absorption, diskbb for a disk black-body, bremss for bremsstrahlung and po for a power law. These types

of radiation are all discussed in section 2.1. Each model has a number of free parameters.

For the disk black-body (diskbb), the free parameters are the temperature of the inner part of the disk in keV (kT_{in}) and a normalization factor ($norm_{disk}$), equal to $(R_{in}/D)^2 \cos(\theta)$. Here R_{in} is the inner disk radius, D is the distance to the object and θ is the angle of the disk with respect to us, 0 is face-on and π is edge-on. For the power law (po), the free parameters are the only variables, as discussed in section 2.1. These are N_0, the intensity of photons at 1 keV and the photon index Γ.

Bremsstrahlung (bremss) also has two free parameters, these are the plasma temperature in keV (kT) and a normalization ($norm_{bremss}$), equal to $\frac{3.02E15}{4\pi D^2} \int n_e n_I dV$. Here D again is the distance to the object. n_e and n_I are the electron and ion densities.

The last model is comptonization (comptt). The free parameters are the temperature of the plasma, again in keV (kT), the optical depth of the plasma (τ) and an overall normalization factor ($norm_{comptt}$).

Every fit includes absorption with a initial value of $7 * 10^{20} cm^{-2}$. This means the software will start searching from that value. This value is chosen because it is the approximate value of absorption between M31 and our galaxy as described in section 2.1. If the flux is mostly a straight line, it is probably a power law. If it drops again at higher energies, it can be bremsstrahlung. These two are sometimes hard to distinguish, so when in doubt both are tried. If the flux rises and then drops again, it is a black-body. Combinations of a black-body with a power law are possible. A black-body can be further altered by comptonization. If the spectrum is not conclusive about the source type, the HR can be used as an indication if it is a hard or soft source. It is important to note that XSpec simply does a mathematical fit. The results have to be checked. They might not be physically possible. After identifying all bright sources (those with over 1000 counts, as discussed in section 3.3), these identification are compared to earlier identifications. For this the NASA/IPAC Extragalactic Database (NED) is used, along with some papers about M31 Surveys. The database shows all known sources around a given coordinate and the relevant papers. This is also used to look for optical counterparts of the sources. Sources that are very different from the other ones are investigated further. These can for example include an extremely bright source, or one that has changed very much between the first and second observations.

4 Results

4.1 Identifications

The first observation contained twelve sources with over 1000 counts. The coordinates of all twelve sources can be found in table 1. In observation 2, the same sources were analyzed again.

Source	Coordinates (RA+DEC)
1	J004251.8+413108
2	J004248.7+412324
3	J004243.4+412408
4	J004259.7+411919
5	J004303.6+411803
6	J004311.0+411447
7	J004221.0+411607
8	J004223.1+411532
9	J004230.6+411620
10	J004238.0+411559
11	J004248.3+411516
12	J004252.2+411539

Table 1: *Elliptical coordinates of all sources with over 1000 counts. The uncertainty in the position is a few arcseconds, as described in section 3.3*

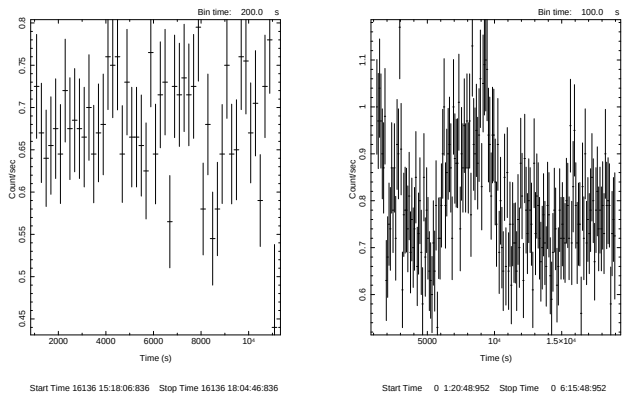

(a) (b)

Figure 6: *Light curves of source 1. There is some variation from 6000s onwards in obs 1 (a), but not very much. Obs 2 (b) shows an increase in brightness between 6000 and 10000s.*

The light curves and PDS for source 1 are shown in figures 6 and 7.

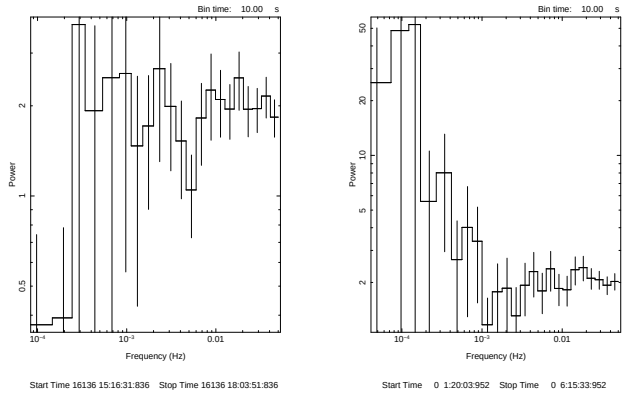

(a) (b)

Figure 7: *PDS of source 1. There is no statistically significant peak in obs 1 (a). Obs 2 (b) shows possible variability around 5E-04 Hz.*

The light curve of obs 1 shows some variation from 6000s onwards. However, the variations are not very large. This is also reflected by the PDS. Some variability is visible, but no variability is statistically very well possible. The calculated F_{var} is -.04, also indicating no variability. The second observation shows much more variation, which is also seen in the PDS. Note the axes have a log scale. The variability indicates this is probably a XRB, and not a GLC.

The fitted spectrum is shown in figure 8. The best fit in obs 1 is a power law with $\chi^2/DOF =$ .97. The values and uncertainties of the parameters are in table 2. The calculated HR is -.04, so the soft and hard fluxes are almost equal. Obs 2 gave similar results.

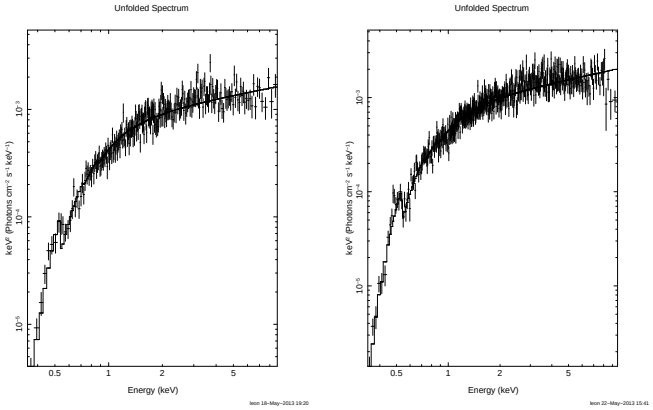

(a) (b)

Figure 8: *Spectra of source 1. A power law with Γ = 1.67(3) is most likely in obs 1 (a). This has decreased a bit to 1.60(2) in obs 2 (b).*

This source was found in the NED database. It has previously been classified by Barnard et al. 2013 [2] as being a BHB. They found a luminosity of 4.5E38. That is well above the Eddington limit for a 2 $M_\odot$ NS. The luminosity is $4.2E38$ in obs 1 and $4.6E38$ in obs 2, similar to what Barnard et al. have found. It is very likely to be a BHB.

Parameter	obs 1	obs 2
n_H	0.36(2)E22	.35(1)E22
Γ	1.67(3)	1.60(2)
N_0	8.0(3)E-04	8.2(2)E-04
χ^2/DOF	.97	1.2
F_{var}	-.04	17.2
HR	-.04	.01

Table 2: *Parameter values for source 1.*

The same analysis procedure was repeated for all twelve bright sources in the field. Most of them are power laws. The results for all sources with just a power law can be found in table 6 for obs 1 and 10 for obs 2. These tables and all other tables with model parameters for all sources can be found in Appendix A. 1σ uncertainties are given in brackets.

The sources with a black-body spectrum, possibly with comptonization can be found in table 7 for obs 1 and 11 for obs 2. The bremsstrahlung source can be found in tables 8 and 12, respectively. Finally the source with a disk black-body and a power law can be found in table 9 and table 13.

The PDS, light curves and spectra of all sources can be found in Appendix B.

All identifications will be discussed briefly, with the exception of the most interesting ones. They have their own subsection.

Source 2 has a power law and has been classified earlier as a XRB [17]. No optical counterpart is known, so it is probably a LMXB. A high mass companion would have a higher luminosity. That would probably be seen. Source 3 has a bright black-body spectrum. It is discussed separately in section 4.2. Source 4 and 5 have similar power law spectra. Both have earlier been associated with a GLC [17]. Source 4 shows very little variability. Source 5 seems to have more, looking at the light curve. However the PDS shows no strong features. Neither source shows significant variability. They could indeed be part of a GLC. Source 6 also has a power law spectrum. It has a quite high luminosity, 1.2E38 ergs/s in obs 1 and 1.3E38 ergs/s in obs 2. This is very bright, but does not yet exceed the Eddington limit for a NS. This source is also associated with a GLC [14] [17]. Source 7 is the only source with a bremsstrahlung spectrum. This indicates a SNR of WD with outbursts. It is also measured by Voss et al. 2007 [20]. There it is only identified as being a point-like source. As SNR are extended, a WD with outbursts is more probable. The light curves and PDS are too poor to measure the outbursts. Source 8 is another bright source, with a luminosity of about 1.5E38 ergs/s. This source has been classified as a BHB by Barnard et al. [1]. A weak optical counterpart has been found, indicating it is a LMXB. The measurements in obs 1 and 2 indicate that the BHB is now in its hard state. as it has only a power law spectrum. Source 9 is a power law source. It has been classified by Pietsch et al. [14] as hard. No distinct time variability is seen. There is not enough information to be ably to classify this source. A best guess would be a XRB. Source 10 has a comptonized disk spectrum in obs 1, but a power law spectrum in obs 2. It is discussed separately in section 4.3. Source 11 is quite bright at 1.5E38 ergs/s in obs 1 and 1.2E38 ergs/s in obs 2. It has a power law spectrum. The light curves show little variation. It is a known object, but could be a XRB, SNR or AGN [14] [16]. Source 12 has a disk with power law spectrum and is discussed separately in section 4.4.

4.2 Source 3: microquasar

Source 3 is located at J004243.4+412408. It has a bright black-body spectrum. The model parameters can be found in table 3. The spectrum is shown in figure 9.

The parameter values have not changed much between observation 1 and observation 2. It is a very bright source, the unabsorbed luminosity is about 1E38 ergs/s in the .3-10 keV range.

It has been extensively examined by Middleton et al. [12]. The parameters as measured by me correspond to those measured by Middleton et al. with the same data. They have also used older observations by XMM-Newton and other instruments

Parameter	obs 1	obs 2
$n_H(10^{22})$	.41(2)	.39(2)
kT_{in}	0.46(1)	.36(1)
$norm_{disk}$	2.59(37)	3.39(63)
$L(10^{37})$	6.9	14
χ^2/DOF	0.8	.9
HR	-.96	-.99
F_{var}	.16	1.06 (100) / 4.49

Table 3: *Parameters of source 3.*

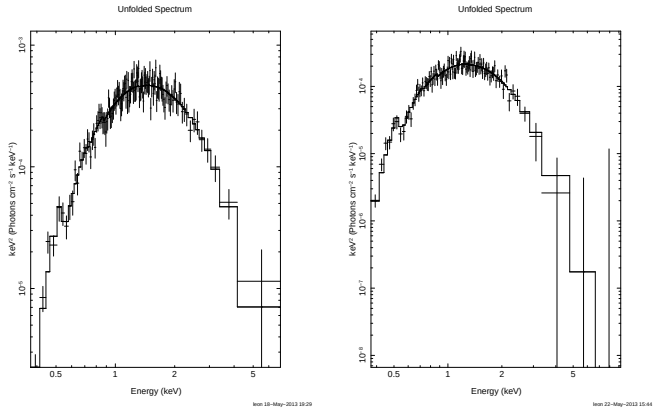

(a) (b)

Figure 9: *Spectra of source 3. It is a very bright black-body. In obs 1 (a) it was brighter than in obs 2 (b)*

to find out more about this source. It has been even brighter, up to 1.3E39 ergs/s. This makes it an ultra luminous X-Ray source (ULX). It is probably a stellar-mass microquasar, the first to be found outside our own galaxy. The accretion rate is very high, explaining the high luminosity.

4.3 Source 10: Z source

This source is probably the most interesting one. It is located at J004238.0+411559. A source has previously been discovered at this position. It has been described by Barnard et al. in 2003 [3]. As

Parameter	obs 1 (comptt)	obs 1 (po)	obs 2
nH	.249(6)E22	.27(4)E22	.12(1)E22
kT_{in}	.110(2)	.105(9)	-
$norm_{disk}$	2.7(3)E03	3.3(30)E03	-
Γ	-	1.86(4)	1.78(5)
N_0	-	1.72(8)E-03	6.9(3)
kT	1.6(1)	-	-
τ	9.1(5)	-	-
$norm_{comptt}$	3.7(2)E-03	-	-
$L(10^{37})$	46	89	
χ^2/DOF	1.1	1.2	1.1
HR	-.39	.35	-.14
F_{var}	-.15	-.15	2.98

Table 4: *Parameter values for source 10.*

this was ten years ago, it is worth checking if the source still behaves as it did back then. Therefore I downloaded more observations from the XMM-Newton archive and analyzed this source for each of them. The parameters for observation 1 and 2 can be found in table 4. The spectra in figure 10. In observation 1, a comptonized disk or a disk with a power law is a good fit. Fitting only a power law gives a χ^2/DOF of 1.2, with a probability of 6.8E-03. The second observation does agree with a power law, with probability .28. This could indicate a BHB or NS that has changed from the soft state to the hard state. All other observations only agree with a disk with a power law. In these observations, the disk is hotter than in observation 1, $\tilde{2}$ keV versus .1 keV. .1 keV is extremely cold for a disk. This is not very realistic.

According to Barnard et al., this source is a Z-Source. These sources are very rare, only nine candidates are known. Its name comes from the shape they draw in a hardness-intensity diagram (HID). See e.g. Lin et al. 2009 [11]. Barnard et al. made a HID for this source. I wanted to place my observations in their diagram to check if it agrees with the rest of the data points. See figure 11. However, the calculated HRs are much higher than those in the diagram, .34 for obs 1 and .66 for obs 2. This

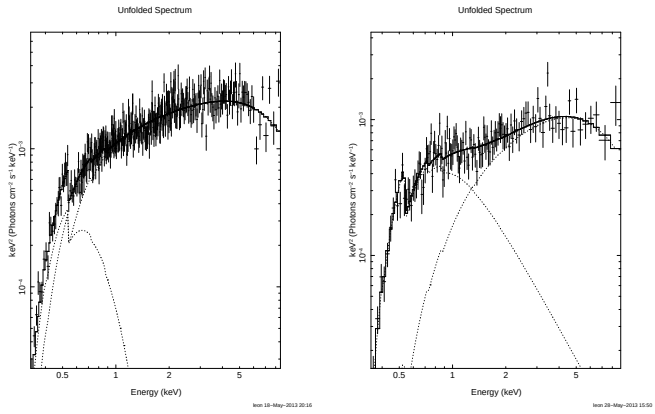

(a) (b)

Figure 10: *Spectra of source 10 in obs 1 (a) and obs 2 (b).*

warrants more research.

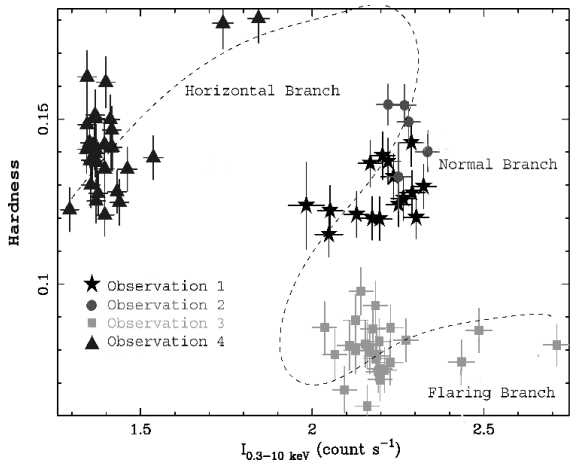

Figure 11: *HID as made by Barnard et al.[3]*

The luminosity of the source was also calculated. It was is 5.6E38 ergs/s during obs 1 and 2.7E38 ergs/s during obs 2. This is brighter than the source [14] was in the observations by Barnard et al. It is even brighter than the Eddington limit for a 2 $M_\odot$ NS. This could mean it is a BHB. However only transient BHBs have ever been observed at these luminosities. This source has been persistently bright for the last decade, as can be seen in the spectra in Appendix C. The conclusion is that it is a super-Eddington NS. This is possible due to a beaming effect. A small portion of the NS produces much more radiation than the rest of the star. When calculating luminosity, uniformity is assumed. This results in a super-Eddington estimate of the luminosity, while the source could be sub-Eddington in reality. This effect is known for BHBs, but has never been proven true in NS. The fact that the luminosity of this source has become even higher than before makes it [17] plausible that the beaming effect also occurs in NS.

4.4 Source 12: super soft source

Source 12 is located at J004252.2+411539. Its parameters can be found in table 5. Notice the large uncertainty in $norm_{disk}$. Also, the power law is very different between the two observations.

Parameter	Value in obs 1	Value in obs 2
$n_H(10^{22})$	9.7(31)	.16(3)
kT_{in}	9.3(8)E-02	7.1(5)E-02
$norm_{disk}$	3.6(28)E03	3.8(30)E4
Γ	1.48(4)	2.67(34)
$N_0(10^{-4})$	.19(7)	.43(8)
$L(10^{37})$	16	10
χ^2/DOF	1.2	.8
HR	-.86	-.97
F_{var}	.35	6.2

Table 5: *Parameters of source 12.*

It has a black-body spectrum with a power law. The spectrum is extremely soft. This is classified as a super soft source (SSS). The spectra for observation 1 and 2 can be found in figure 12.

This source has also be identified recently by Trudolyubov et al. [18]. They also say it has a very soft black-body, with $T_{in} < 100eV$, with a power law with varying Γ. The data quality is not good enough to determine if the variability discovered by Trudolyubov et al. is still there. Assuming it

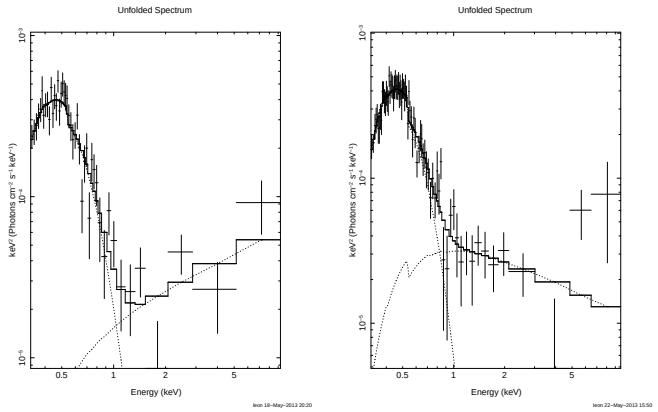

(a) (b)

Figure 12: *Spectra of source 12 in obs 1 (a) and obs 2 (b).*

is really there, this source is probably an accreting white dwarf with constant hydrogen burning on the surface.

5 Conclusion

This bachelor project has allowed me to take a look in the 'real' scientist world. I learned a lot about the practical aspects of X-Ray spectroscopy, such as dealing with problems that do no arise in normal, theoretical courses. These include low data quality and effects such as flaring that degrade the data. It was nice to be able to use new data. This allowed me to detect possible new things, which may have happened with the Z source. I hope this report reflects the effort and enthusiasm put into it.

knowledge.

6 References

[1] R. Barnard, M. R. Garcia, and S. S. Murray. Reinstating the M31 X-Ray System RX J0042.3+4115 as a Black Hole X-Ray Binary and Compelling Evidence for an Extended Corona. *ApJ*, 743:185, December 2011.

[2] R. Barnard, M. R. Garcia, and S. S. Murray. Chandra Identification of 26 New Black Hole Candidates in the Central Region of M31. *ApJ*, 770:148, June 2013.

[3] R. Barnard, U. Kolb, and J. P. Osborne. Tracing a Z-track in the M 31 X-ray binary RX J0042.6+4115. *A&A*, 411:553–557, December 2003.

[4] M. Cropper. The Polars. *SSR*, 54:195–295, December 1990.

[5] J. M. Dickey and F. J. Lockman. H I in the Galaxy. *ARAA*, 28:215–261, 1990.

[6] C. Done. Observational characteristics of accretion onto black holes. *ArXiv e-prints*, August 2010.

[7] C. Done, M. Gierliński, and A. Kubota. Modelling the behaviour of accretion flows in X-ray binaries. Everything you always wanted to know about accretion but were afraid to ask. *A&AR*, 15:1–66, December 2007.

[8] R. Edelson, T. J. Turner, K. Pounds, S. Vaughan, A. Markowitz, H. Marshall, P. Dobbie, and R. Warwick. X-Ray Spectral Variability and Rapid Variability of the Soft X-Ray Spectrum Seyfert 1 Galaxies Arakelian 564 and Ton S180. *ApJ*, 568:610–626, April 2002.

[9] ESA. EPIC external 'flaring' background. `http://xmm.esac.esa.int/external/xmm_user_support/documentation/uhb_2.1/node34.html`.

[10] ESA. On-axis PSF.

[11] D. Lin, R. A. Remillard, and J. Homan. Spectral States of XTE J1701 - 462: Link Between Z and Atoll Sources. *ApJ*, 696:1257–1277, May 2009.

[12] M. J. Middleton, J. C. A. Miller-Jones, S. Markoff, R. Fender, M. Henze, N. Hurley-Walker, A. M. M. Scaife, T. P. Roberts, D. Walton, J. Carpenter, J.-P. Macquart, G. C. Bower, M. Gurwell, W. Pietsch, F. Haberl, J. Harris, M. Daniel, J. Miah, C. Done, J. S. Morgan, H. Dickinson, P. Charles, V. Burwitz, M. Della Valle, M. Freyberg, J. Greiner, M. Hernanz, D. H. Hartmann, D. Hatzidimitriou, A. Riffeser, G. Sala, S. Seitz, P. Reig, A. Rau, M. Orio, D. Titterington, and K. Grainge. Bright radio emission from an ultraluminous stellar-mass microquasar in M 31. *Nature*, 493:187–190, January 2013.

[13] T. Muñoz-Darias, S. Motta, and T. M. Belloni. Fast variability as a tracer of accretion regimes in black hole transients. *MNRAS*, 410:679–684, January 2011.

[14] W. Pietsch, M. Freyberg, and F. Haberl. An XMM-Newton survey of M 31. *A&A*, 434:483–496, May 2005.

[15] R. A. Remillard and J. E. McClintock. X-Ray Properties of Black-Hole Binaries. *ARAA*, 44:49–92, September 2006.

[16] H. Stiele, W. Pietsch, F. Haberl, and M. Freyberg. Time variability of X-ray sources in the M 31 centre field. *A&A*, 480:599–610, March 2008.

[17] H. Stiele, W. Pietsch, F. Haberl, D. Hatzidimitriou, R. Barnard, B. F. Williams, A. K. H. Kong, and U. Kolb. The deep XMM-Newton Survey of M 31. *A&A*, 534:A55, October 2011.

[18] S. P. Trudolyubov and W. C. Priedhorsky. XMM-Newton Discovery of 217 s Pulsations in the Brightest Persistent Supersoft X-Ray Source in M31. *ApJ*, 676:1218–1225, April 2008.

[19] S. Vaughan, R. Edelson, R. S. Warwick, and P. Uttley. On characterizing the variability properties of X-ray light curves from active galaxies. *MNRAS*, 345:1271–1284, November 2003.

[20] R. Voss and M. Gilfanov. A study of the population of LMXBs in the bulge of M31. *A&A*, 468:49–59, June 2007.

7 Appendix A

7.1 Observation 1

Tables with parameter values for all twelve sources in observation 1.

Source	F_{var}	HR	$n_H(10^{22})$	Γ	$N_0(10^{-4})$	$L(10^{37})$	χ^2/DOF
1	-.04	-.08	.36(2)	1.67(3)	7.96(28)	46	1.0
2	.14	-.03	.49(5)	1.65(7)	1.80(16)	8.7	1.1
4	.23	-.19	.19(4)	1.85(10)	1.20(12)	5.3	1.2
5	.45	-.07	.13(3)	1.70(9)	1.44(12)	5.6	1.2
6	.19	.13	.01(5)	1.45(8)	1.97(14)	12	1.2
8	.16	-.32	.21(3)	2.01(8)	3.58(26)	1.6	1.2
9	.38	-.22	.14(3)	1.88(10)	1.75(15)	9.0	.7
11	.25	-.36	.13(2)	2.06(8)	3.20(20)	15	1.2

Table 6: *Parameter values of the power law sources in obs 1.*

Source	F_{var}	HR	$n_H(10^{22})$	kT_{in}	$norm_{disk}$	kT	τ	$norm_{comptt}$	$L(10^{37})$	χ^2/DOF
3	.16	-.96	.41(2)	.45(1)	2.59(37)	-	-	-	6.9	.8
10	-.15	-.39	.249(6)	.110(2)	2.7(3)E03	1.59(11)	9.15(48)	3.65(20) E-03	46	1.1

Table 7: table
Parameter values of the black-body sources in obs 1. Source 3 has no comptonization, source 10 does have significant comptonization.

Source	F_{var}	HR	$n_H(10^{22})$	kT	$norm_{bremss}$	$L(10^{37})$	χ^2/DOF
7	-.72	-.36	.28(6)	3.59(79)	1.6(2)E-04	5.2	.3

Table 8: *Parameter values of the bremsstrahlung source in obs 1.*

Source	F_{var}	HR	$n_H(10^{22})$	kT_{in}	$norm_{disk}$	Γ	$N_0(10^{-4})$	$L(10^{37})$	χ^2/DOF
12	.35	-.86	9.73(3)	9.27(77)E-02	3.6(28)E03	1.48(37)	1.91(71)E-01	16	1.2

Table 9: *Parameter values of the disk black-body with power law source in obs 1.*

7.2 Observation 2

Tables with parameter values for all twelve sources in observation 2.

Source	F_{var}-100	F_{var}-400	HR	$n_H(10^{22})$	Γ	$N_0(10^{-4})$	$L(10^{37})$	χ^2/DOF
1	2.19	17.2	.01	.35(1)	1.60(2)	8.25(20)	42	1.2
2	1.27	6.42	-.30	.56(4)	1.99(7)	2.08(42)	9.6	.6
4	.80	2.62	-.21	.14(2)	1.88(8)	1.170(78)	5.5	1.0
5	1.97	5.41	-.10	.09(2)	1.73(8)	1.107(79)	7.4	1.3
6	1.13	4.47	.14	.07(2)	1.45(7)	1.82(12)	13	1.3
8	.88	3.79	-.02	.16(2)	1.64(6)	3.01(16)	1.5	.8
9	.86	4.56	-.32	.14(2)	2.01(7)	2.16(12)	7.9	1.3
10	.97	2.98	-.14	.12(1)	1.78(5)	6.9(3)	89	1.1

Table 10: *Parameter values of the power law sources in observation 2.*

Source	F_{var}-100	F_{var}-400	HR	$n_H(10^{22})$	kT_{in}	$norm_{disk}$	$L(10^{37})$	χ^2/DOF
3	1.06	4.49	-.99	.39(2)	.36(1)	3.39(63)	14	.9

Table 11: *Parameter values of the black-body source in observation 2.*

Source	F_{var}-100	F_{var}-400	HR	$n_H(10^{22})$	kT	$norm_{bremss}$	$L(10^{37})$	χ^2/DOF
7	1.05	2.64	-.32	.40(8)	3.9(9)	1.7(2)E-04	4.6	.8

Table 12: *Parameter values of the bremsstrahlung source in obs 2.*

Source	F_{var}-100	F_{var}-400	HR	$n_H(10^{22})$	kT_{in}	$norm_{disk}$	Γ	$N_0(10^{-4})$	$L(10^{37})$	χ^2/DOF
12	1.35	6.20	-.97	.15(3)	7.1(5)E-02	3.7(30)E04	2.66(34)	4.3(9)E-05	10	.78

Table 13: *Parameter values of the disk black-body with power law source in obs 2.*

8 Appendix B

Light curves, PDS and spectra of all twelve bright sources in the first and second observations.

8.1 Observation 1

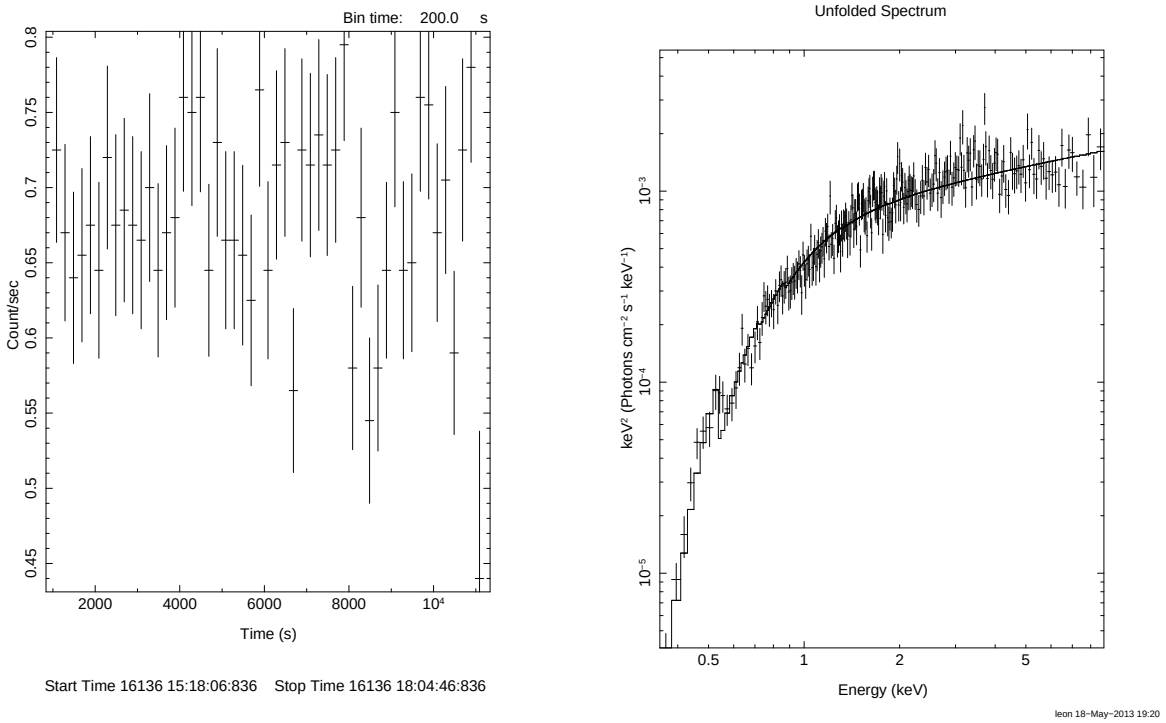

Figure 1: src01: po

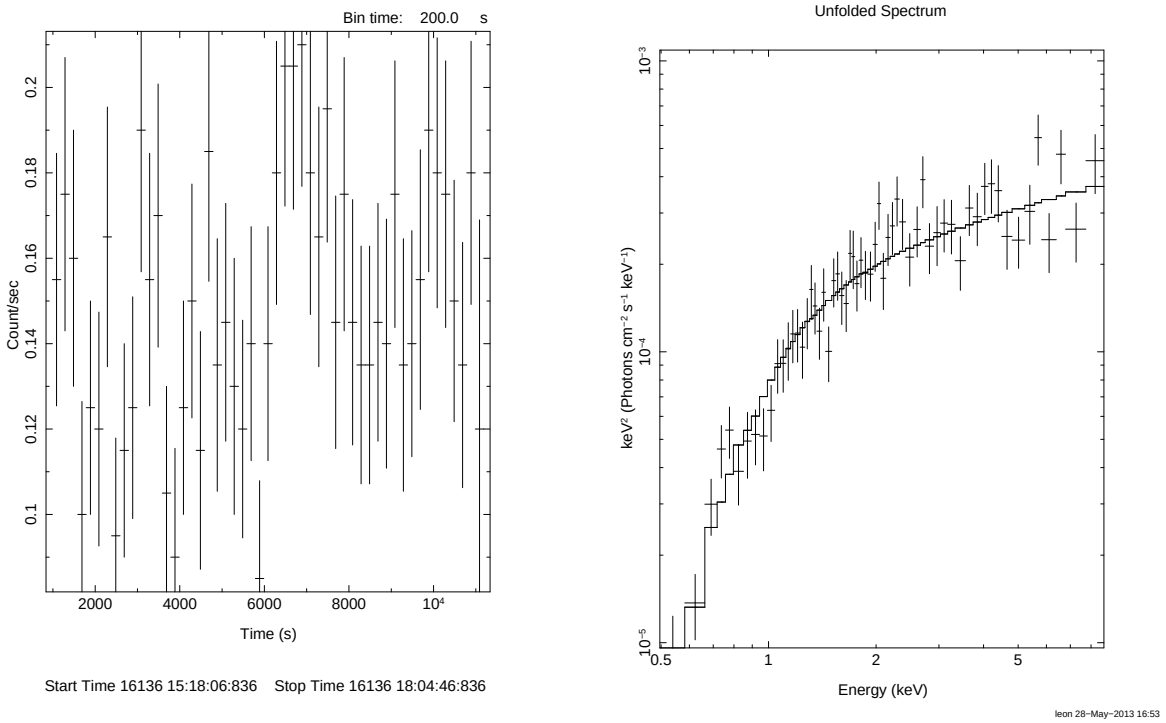

Figure 2: src02: po

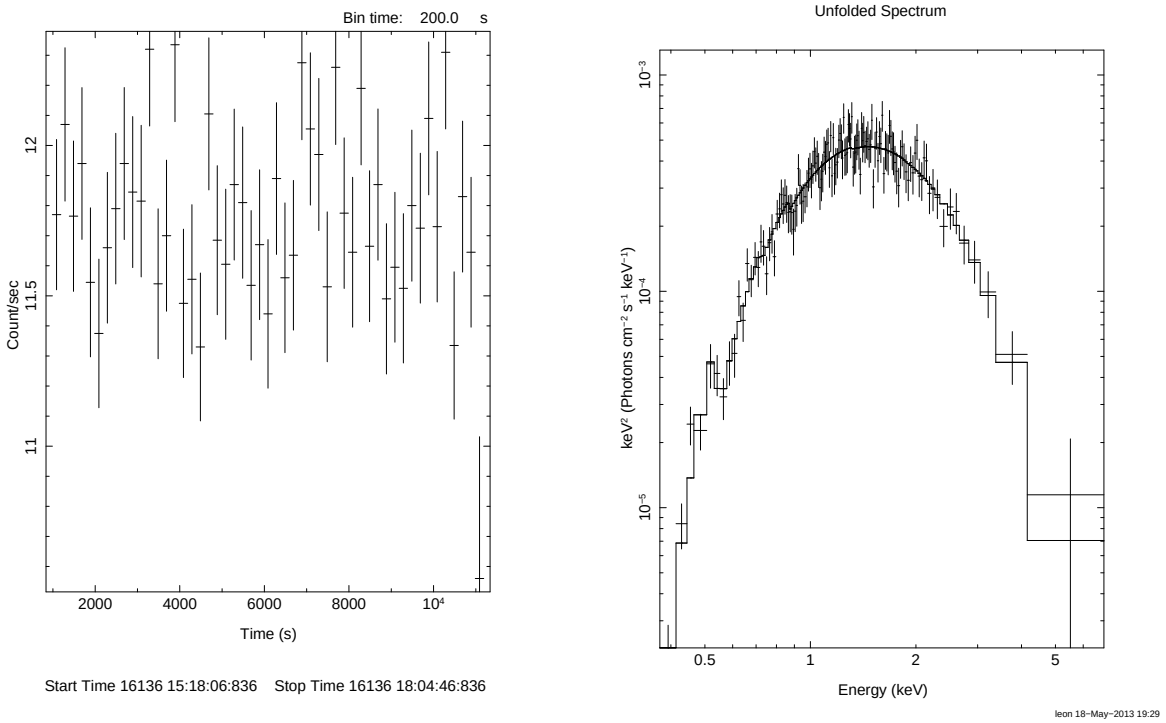

Figure 3: src03: diskbb

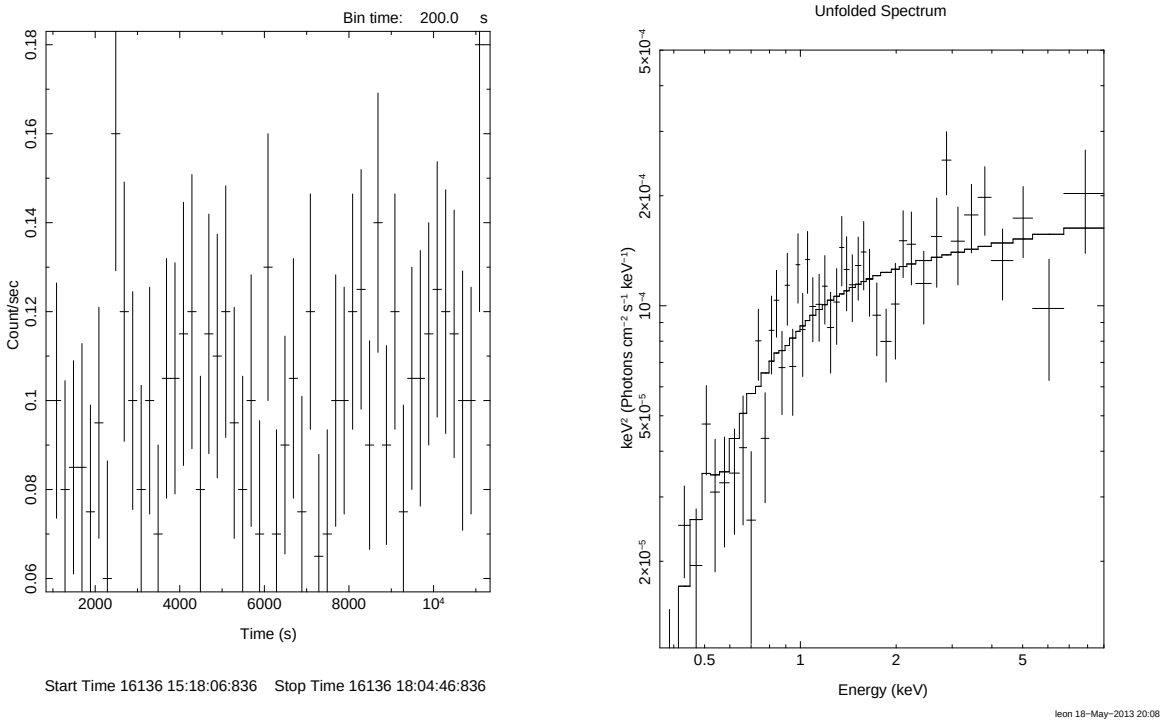

Figure 4: src04: po

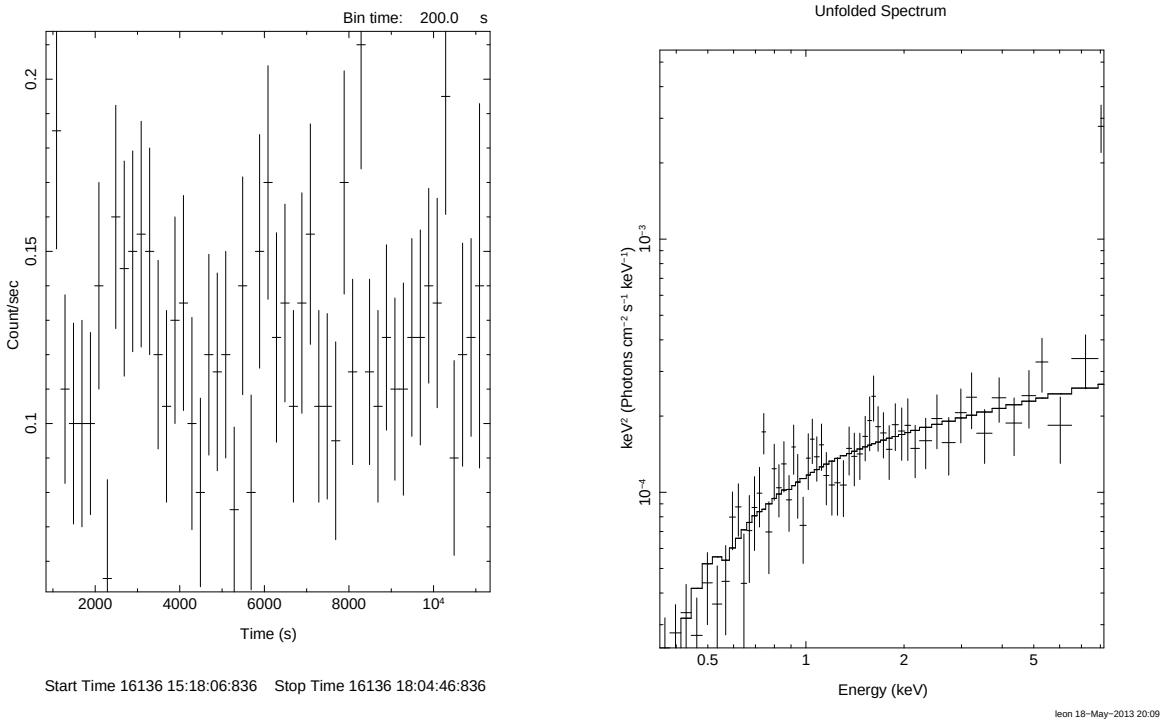

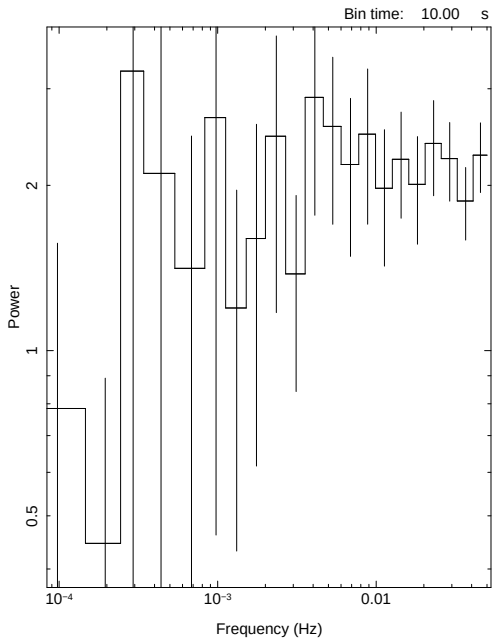

Figure 5: src05: po

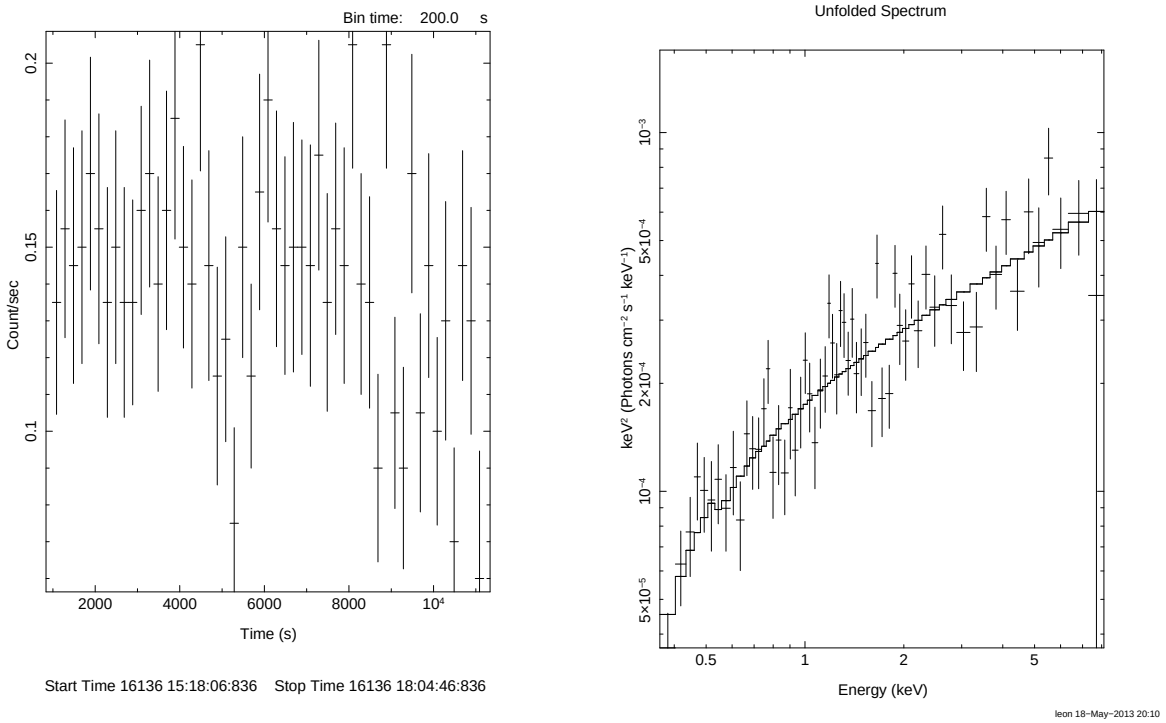

Figure 6: src06: po

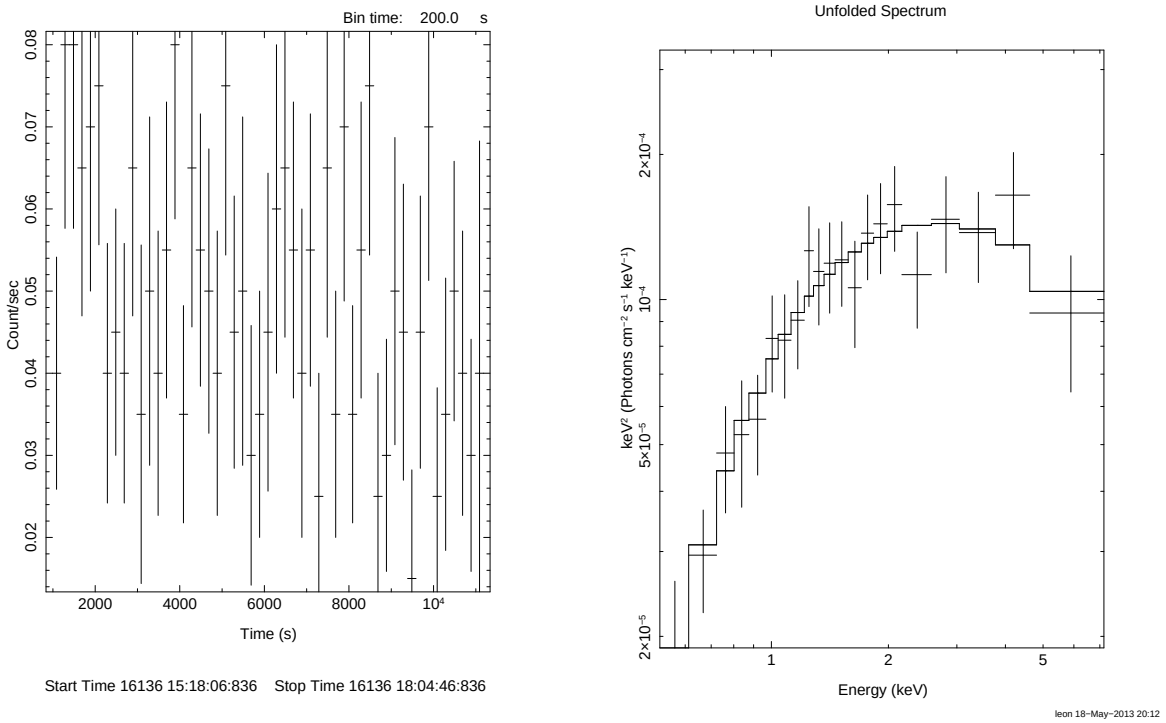

Figure 7: src07: bremss

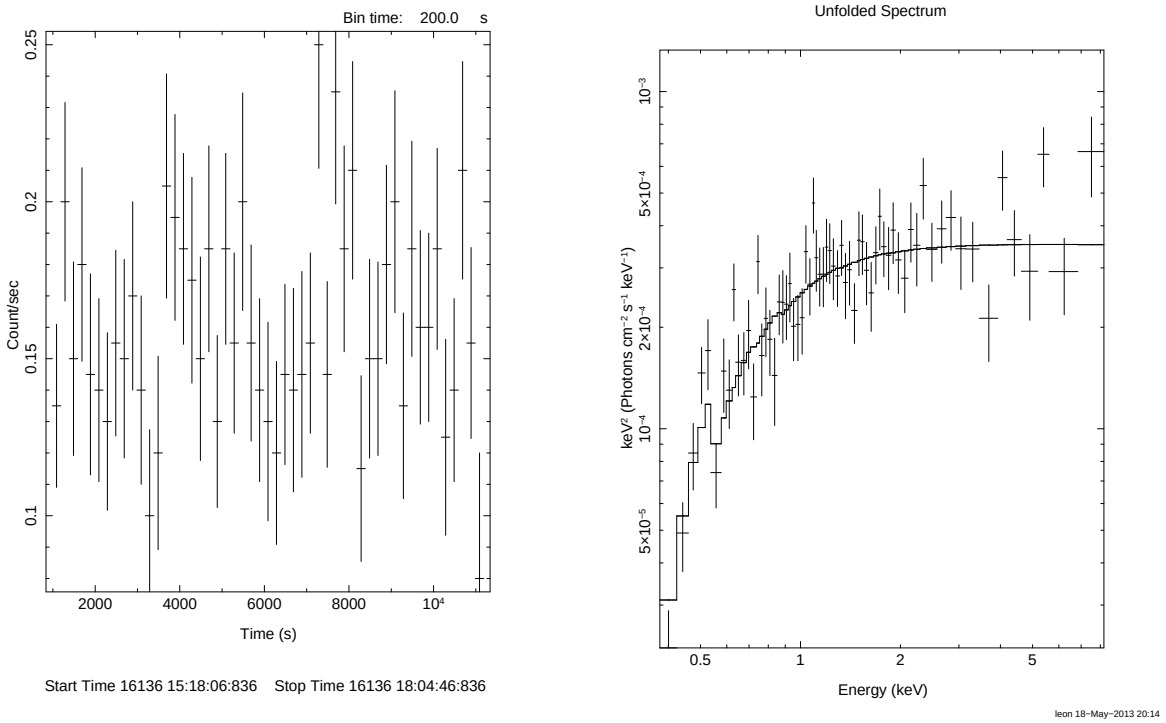

Figure 8: src08: po

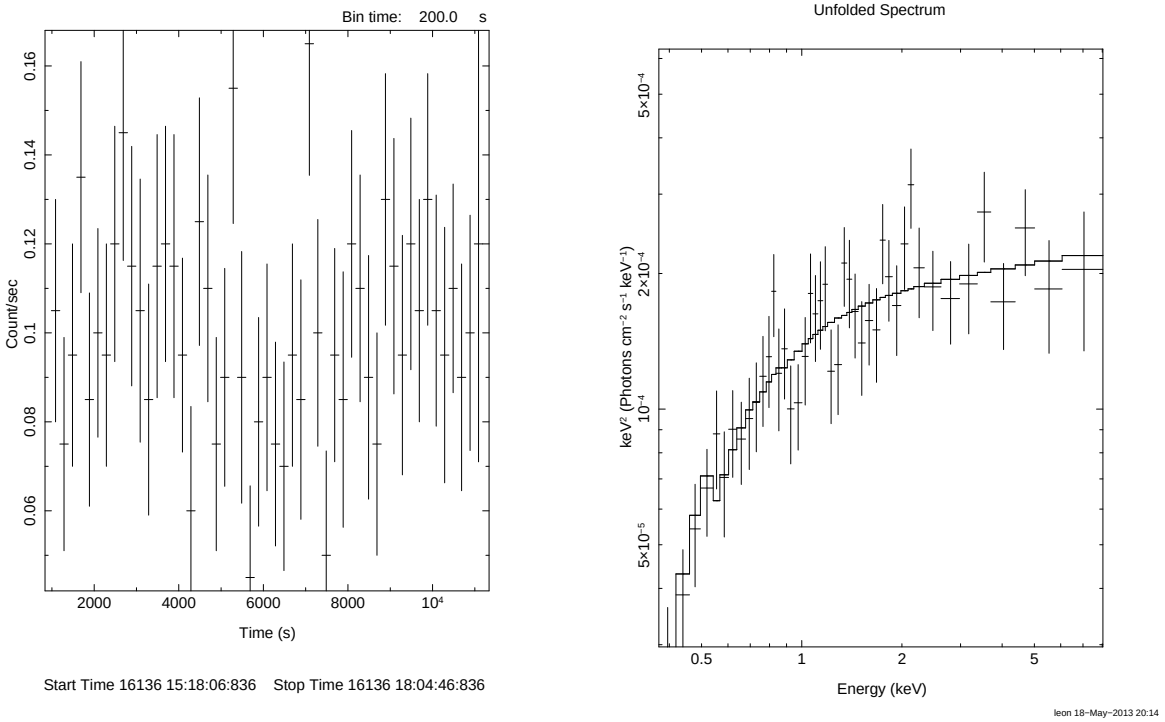

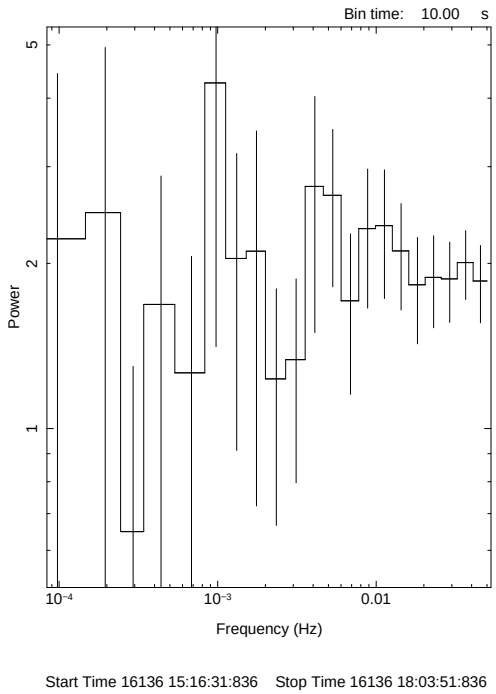

Figure 9: src09: po

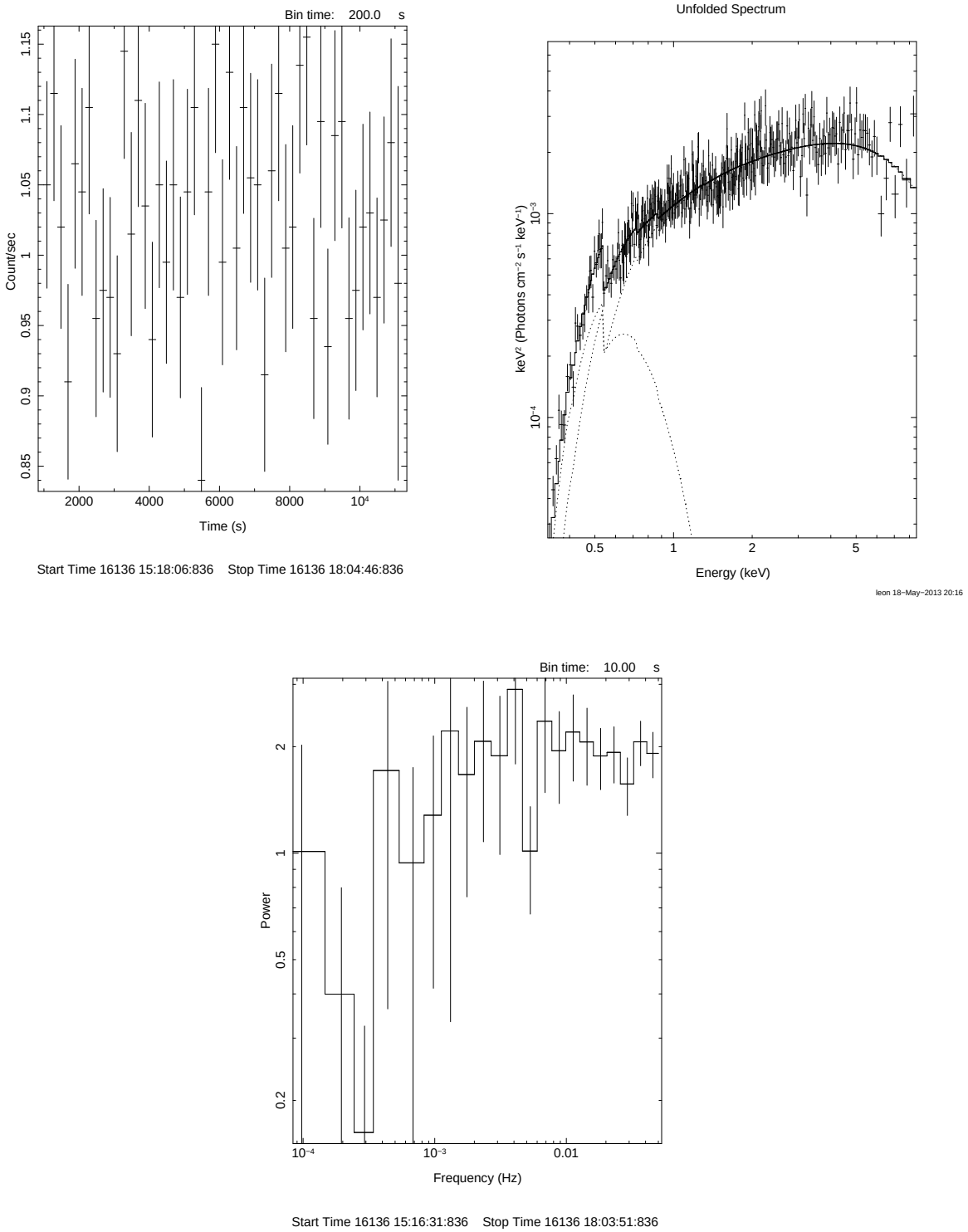

Figure 10: src10: diskbb+comptt

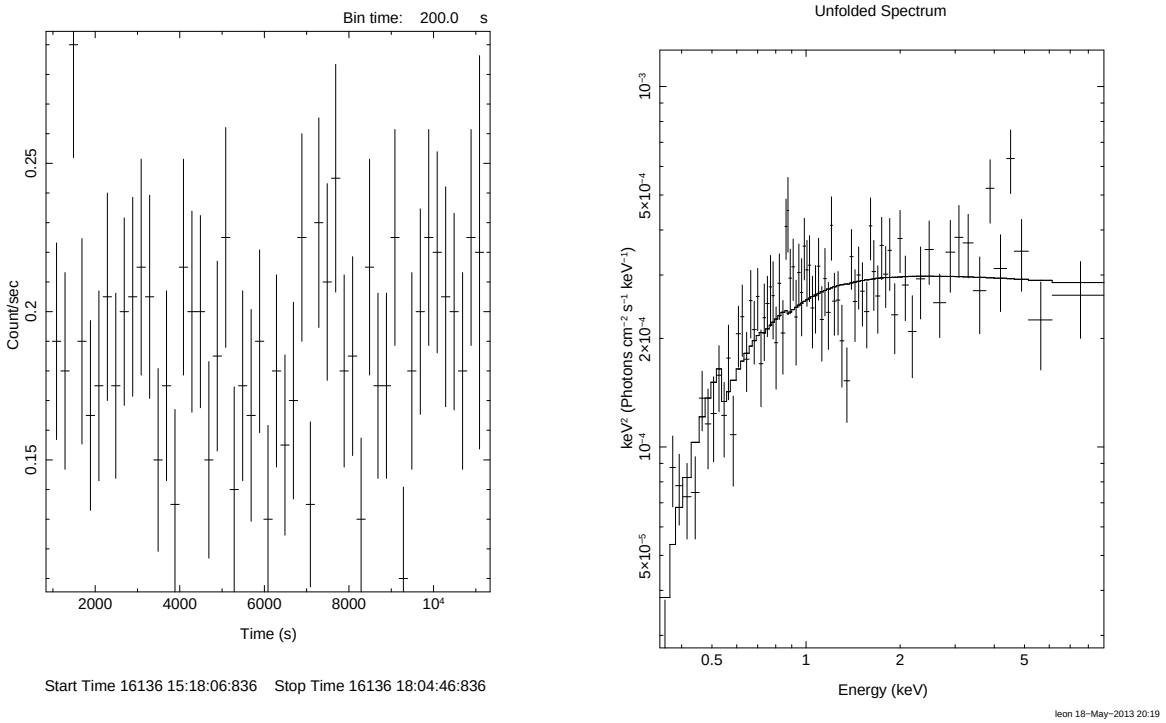

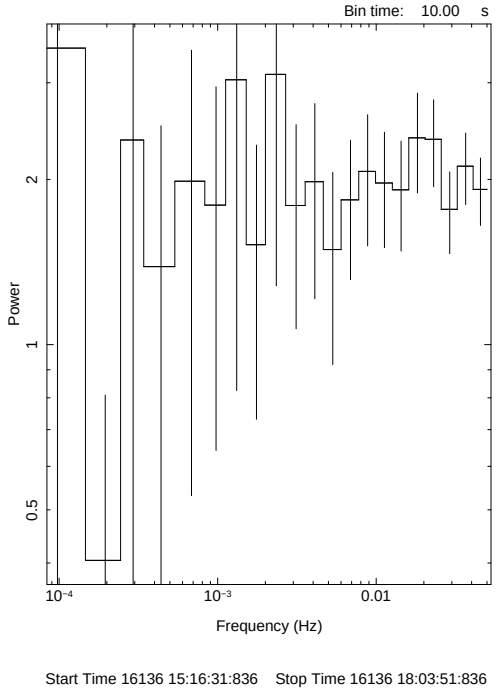

Figure 11: src11: po

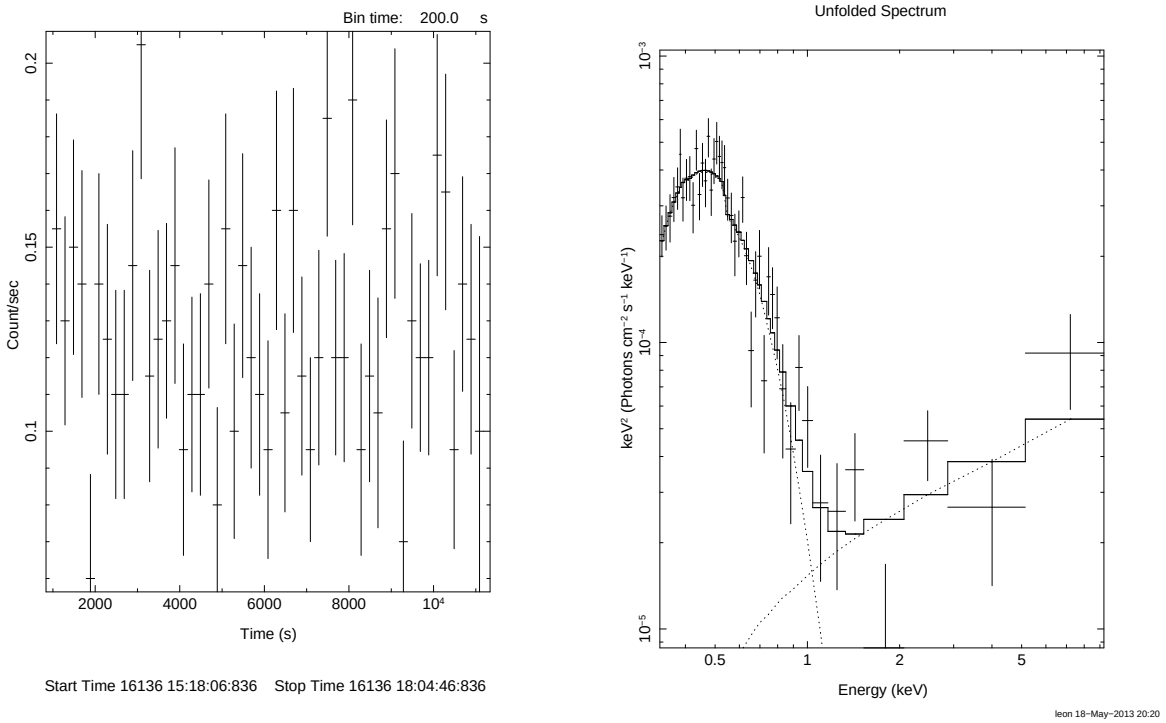

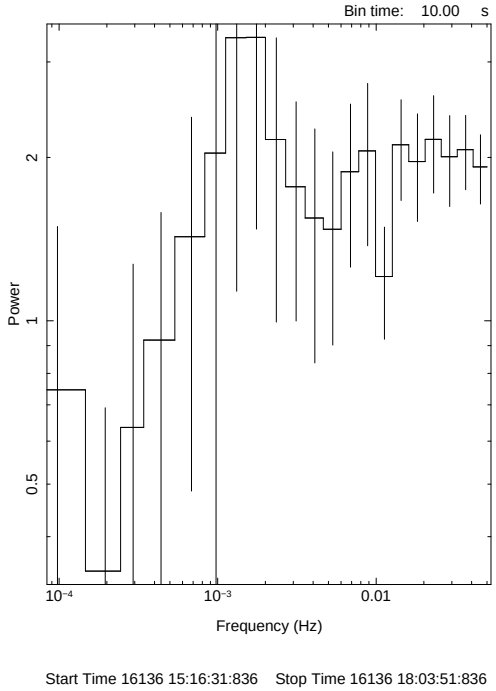

Figure 12: src12: diskbb+po

8.2 Observation 2

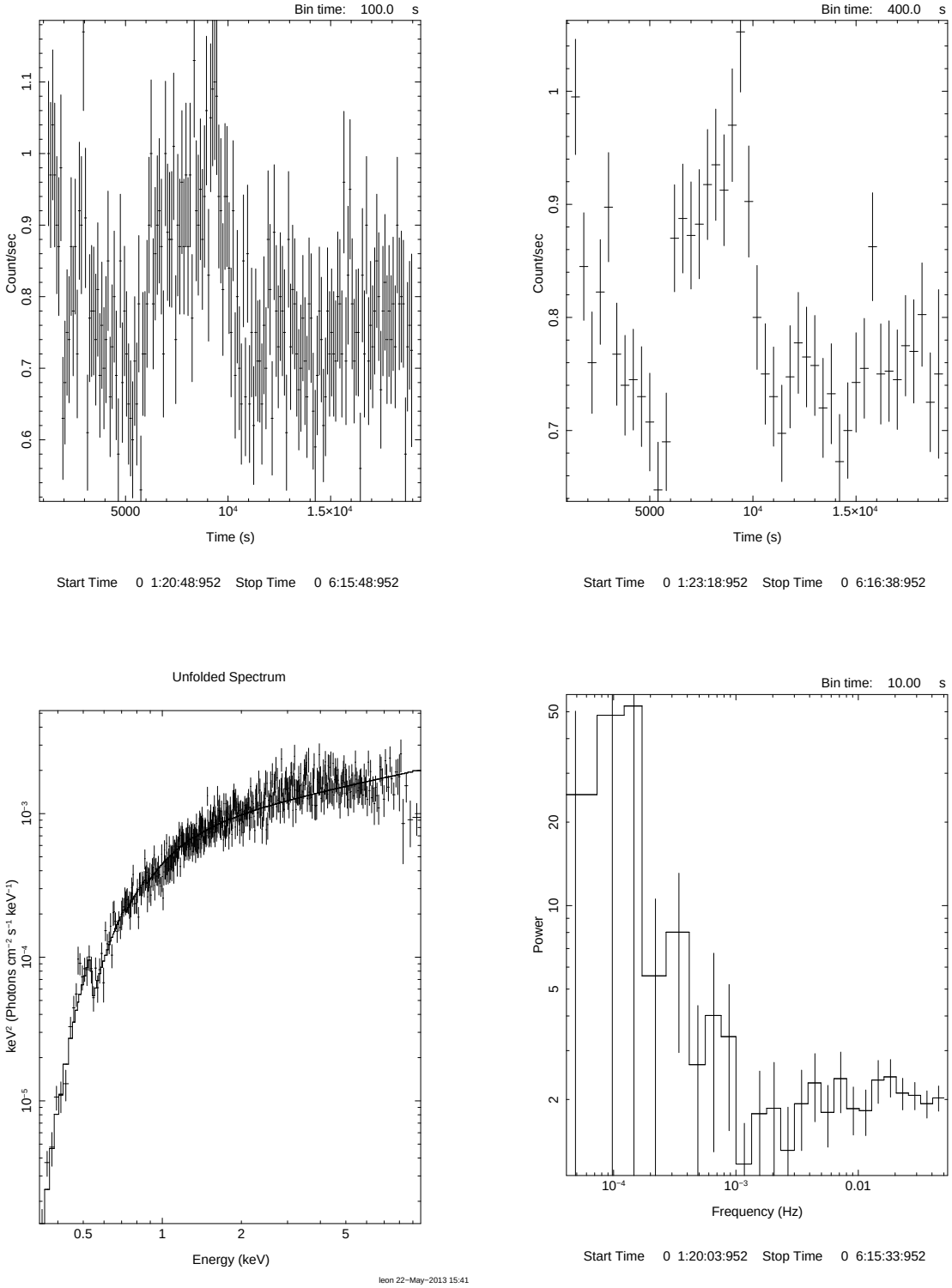

Figure 1: src01: po

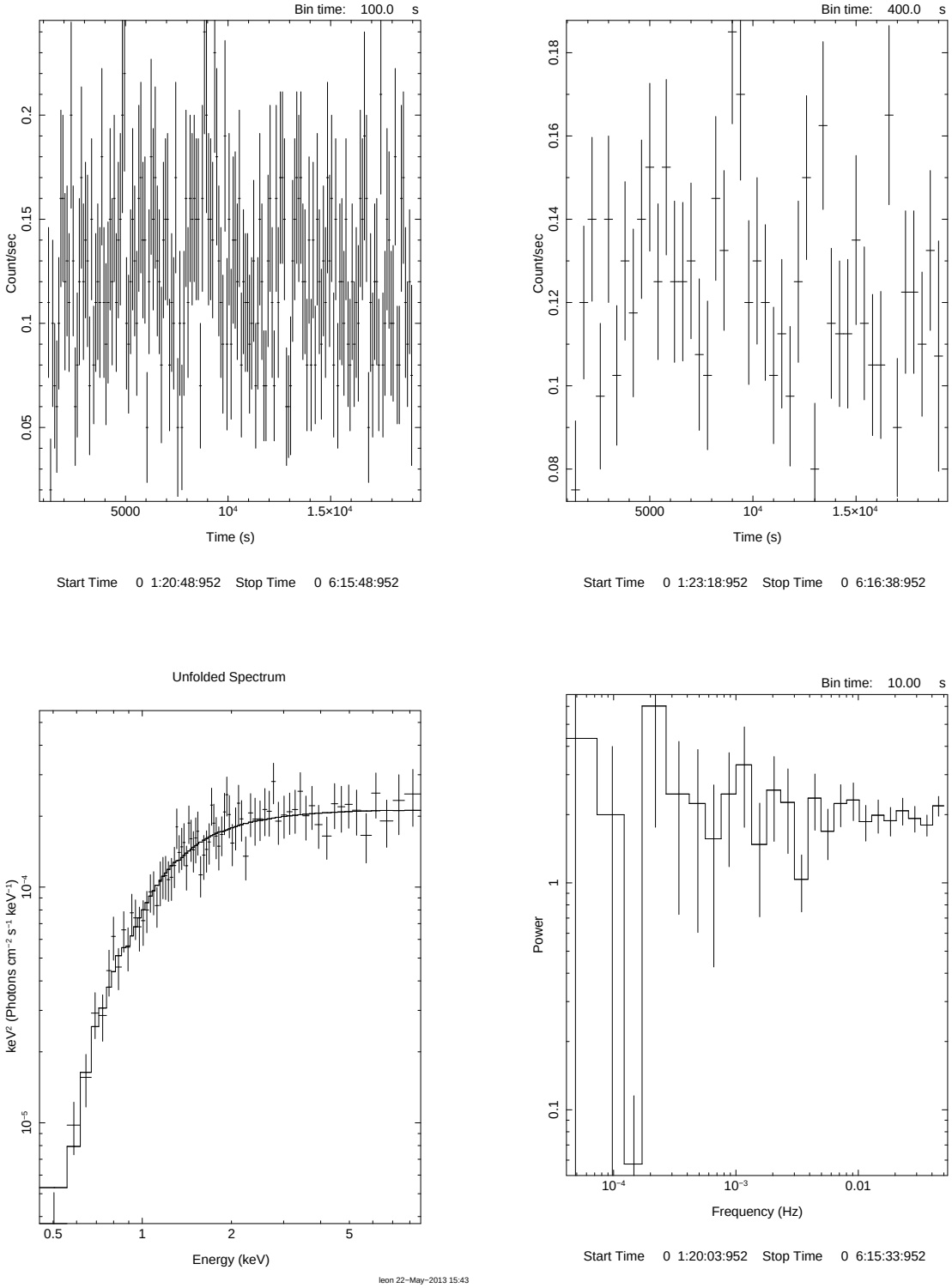

Figure 2: src02: po

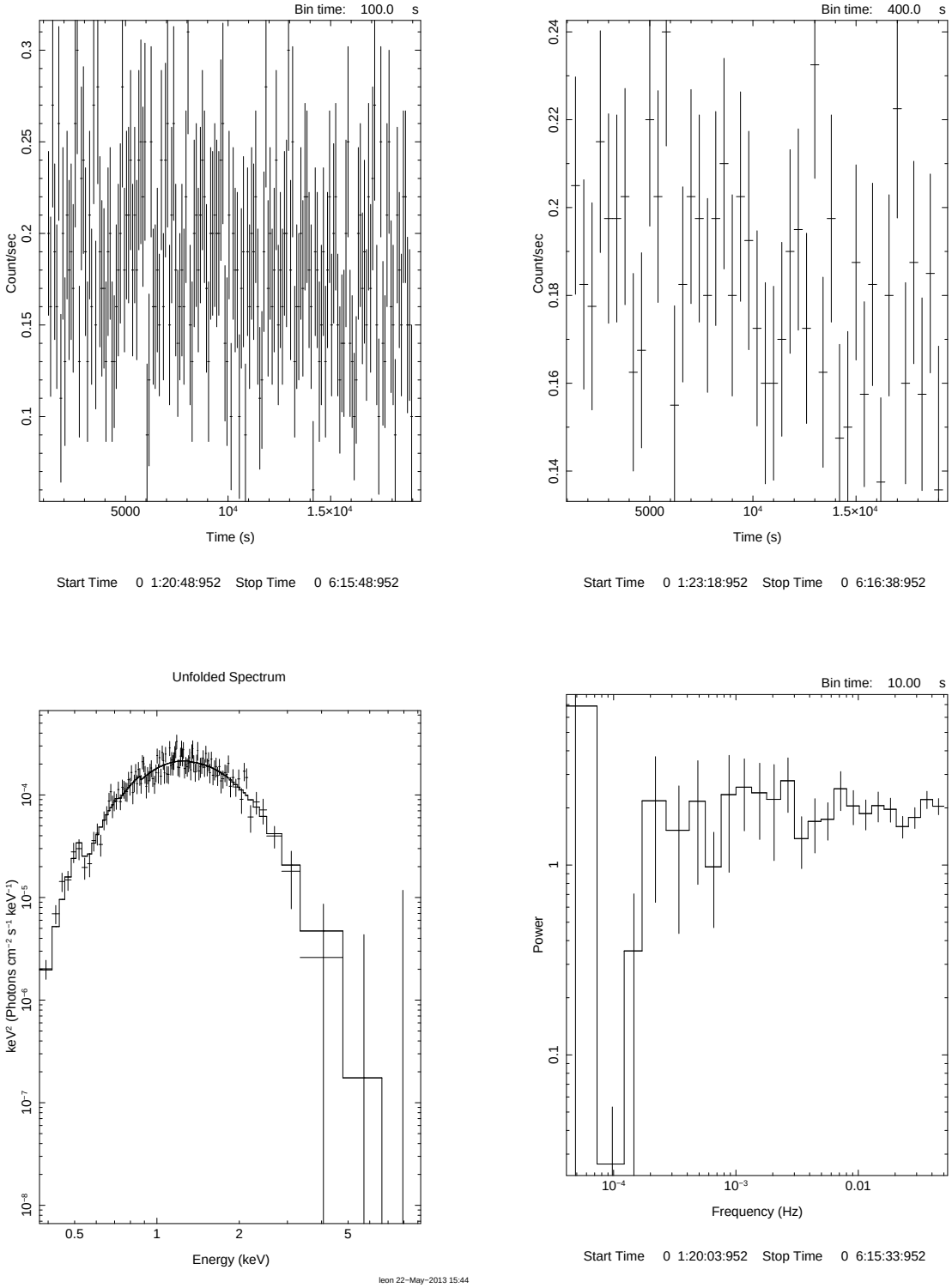

Figure 3: src03: diskbb

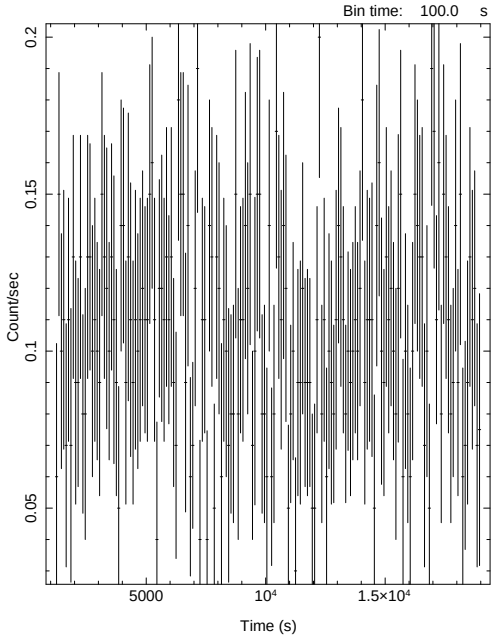

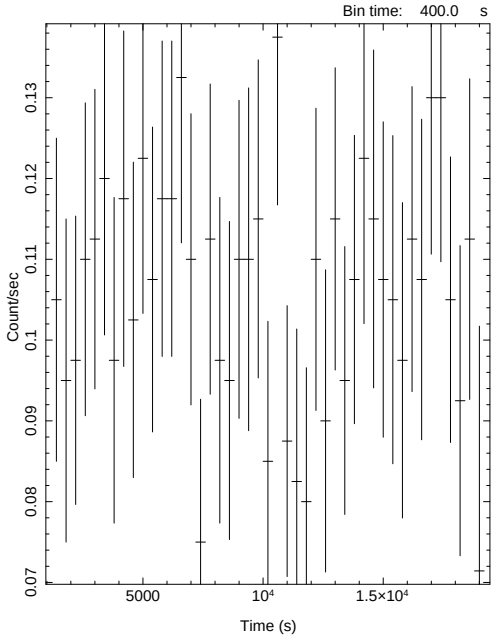

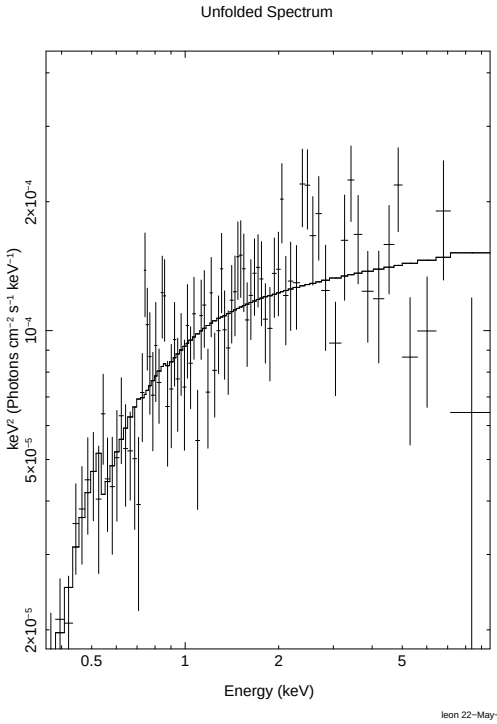

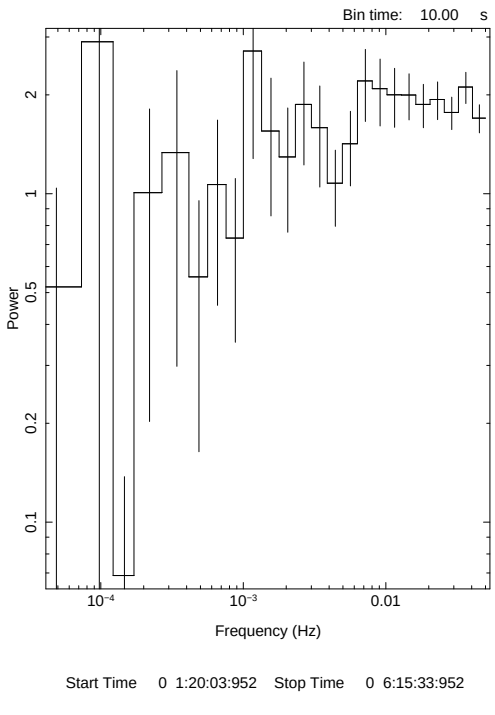

Figure 4: src04: po

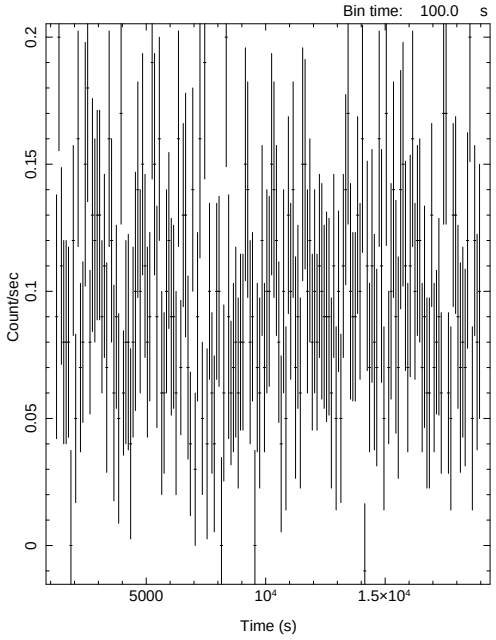

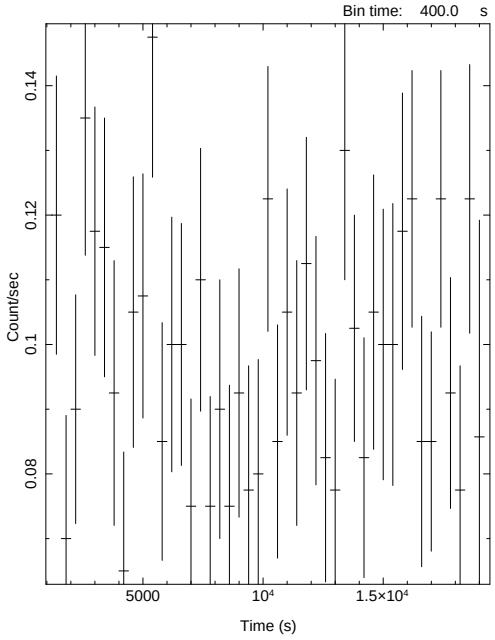

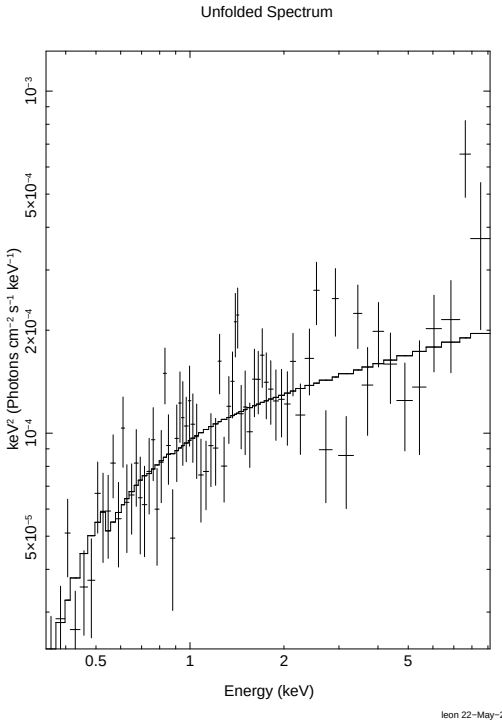

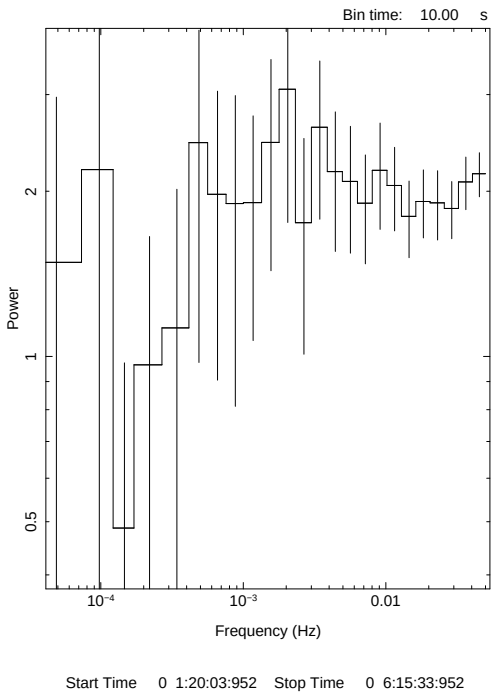

Figure 5: src05: po

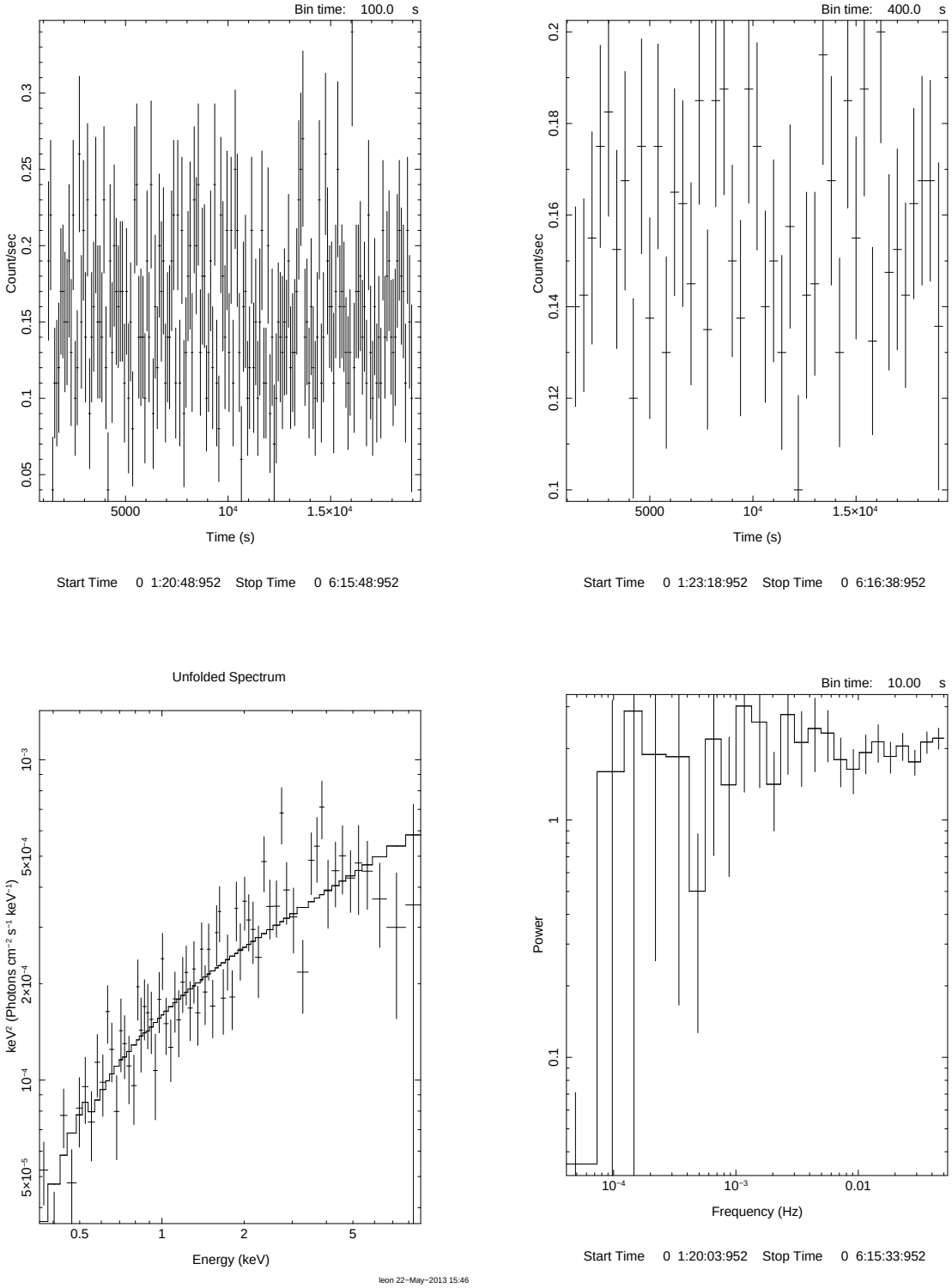

Figure 6: src06: po

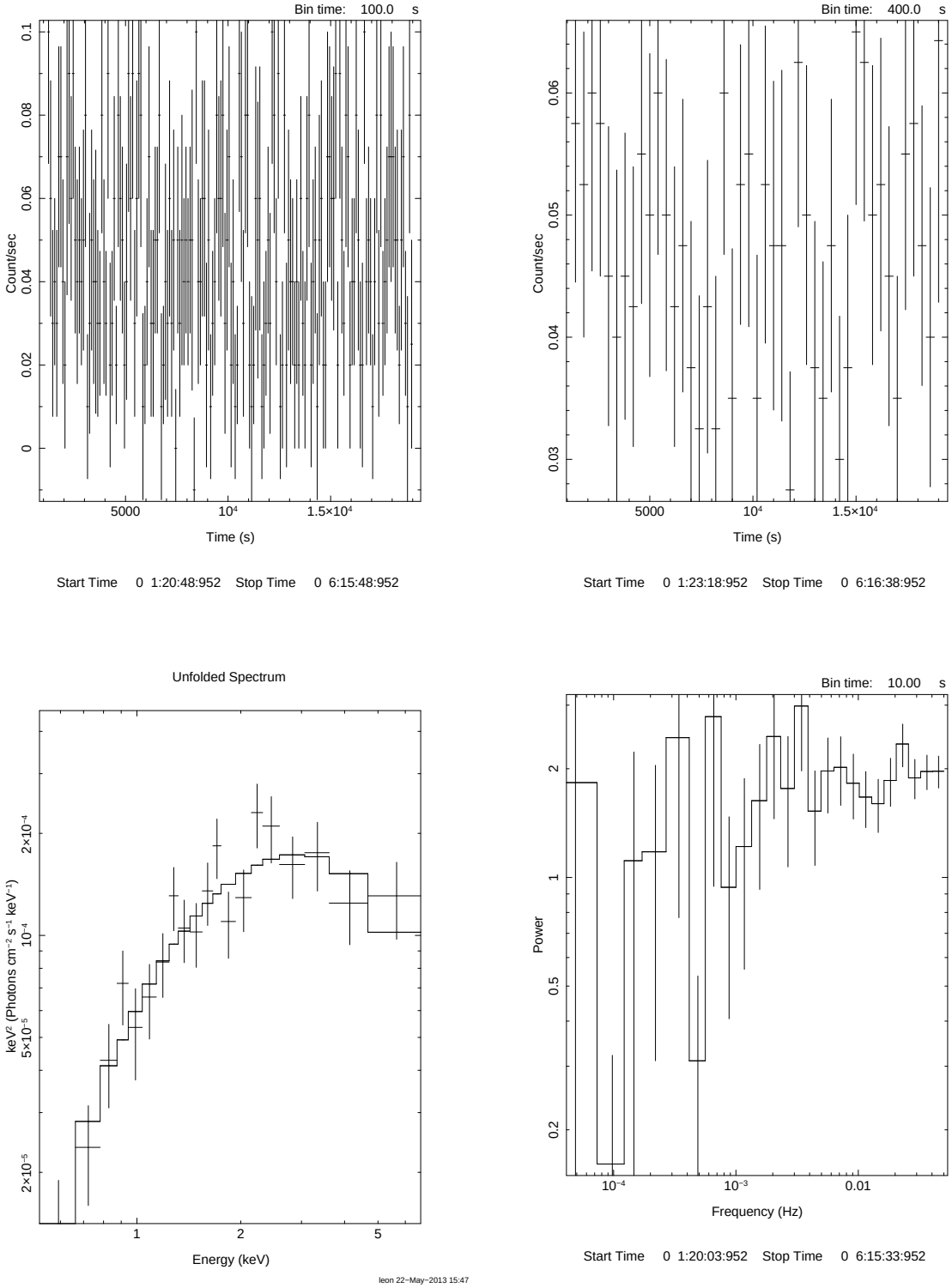

Figure 7: src07: bremss

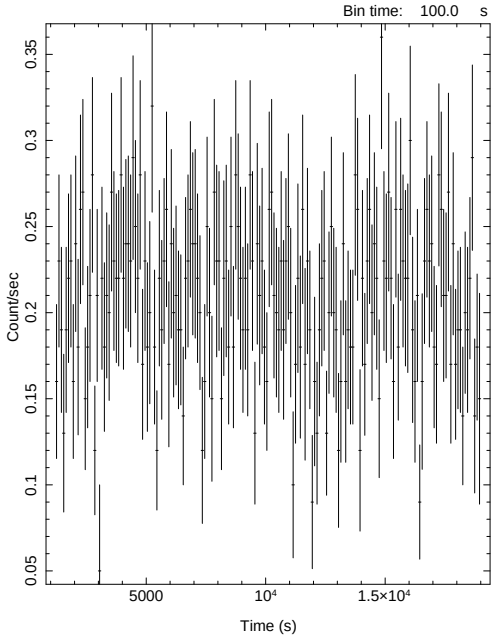

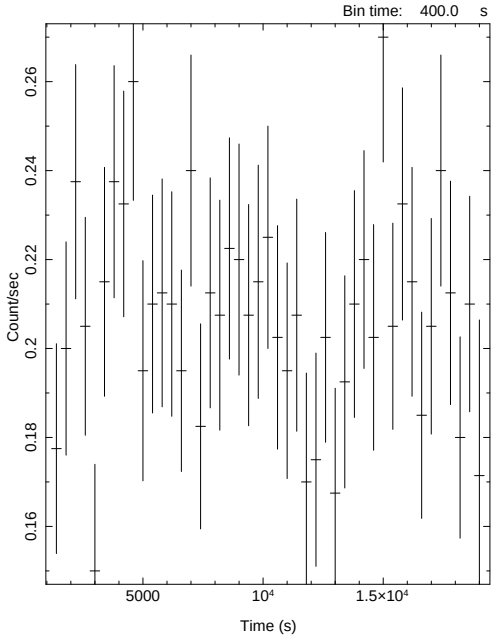

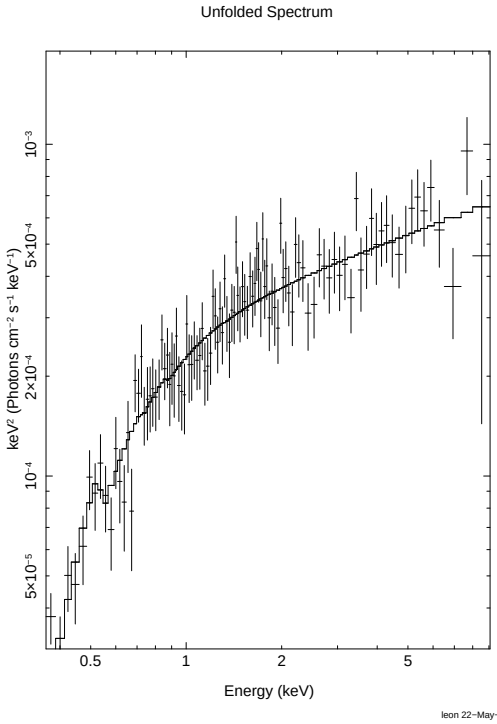

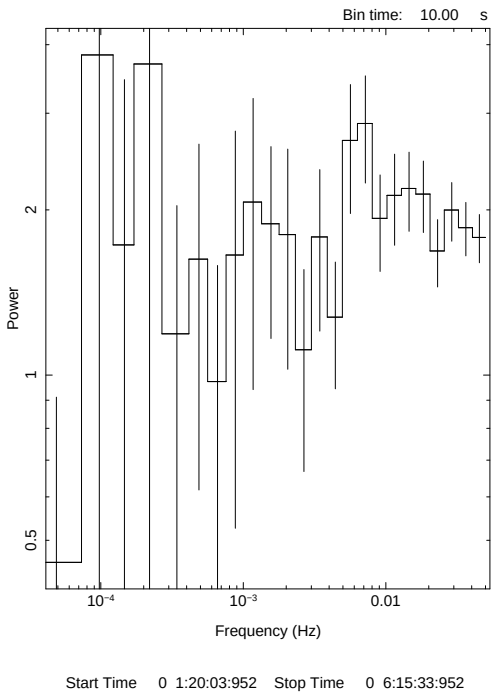

Figure 8: src08: po

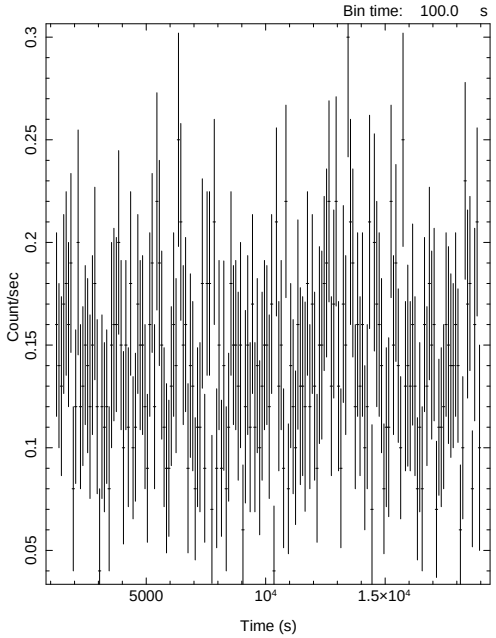

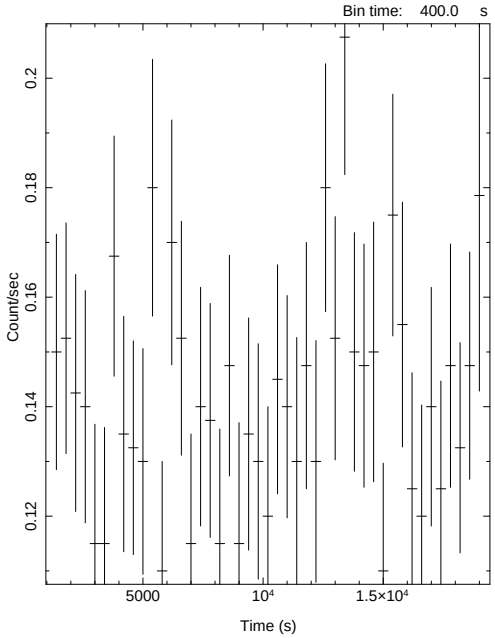

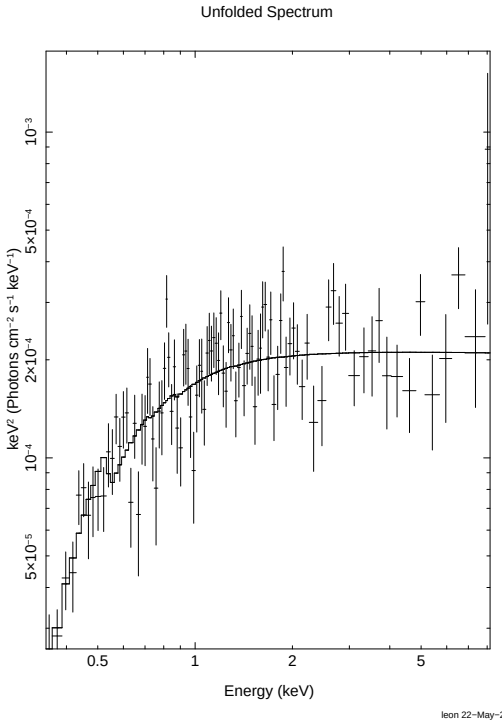

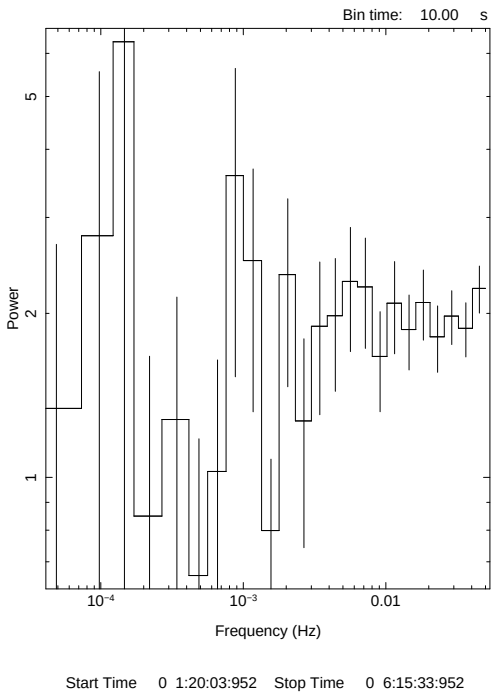

Figure 9: src09: po

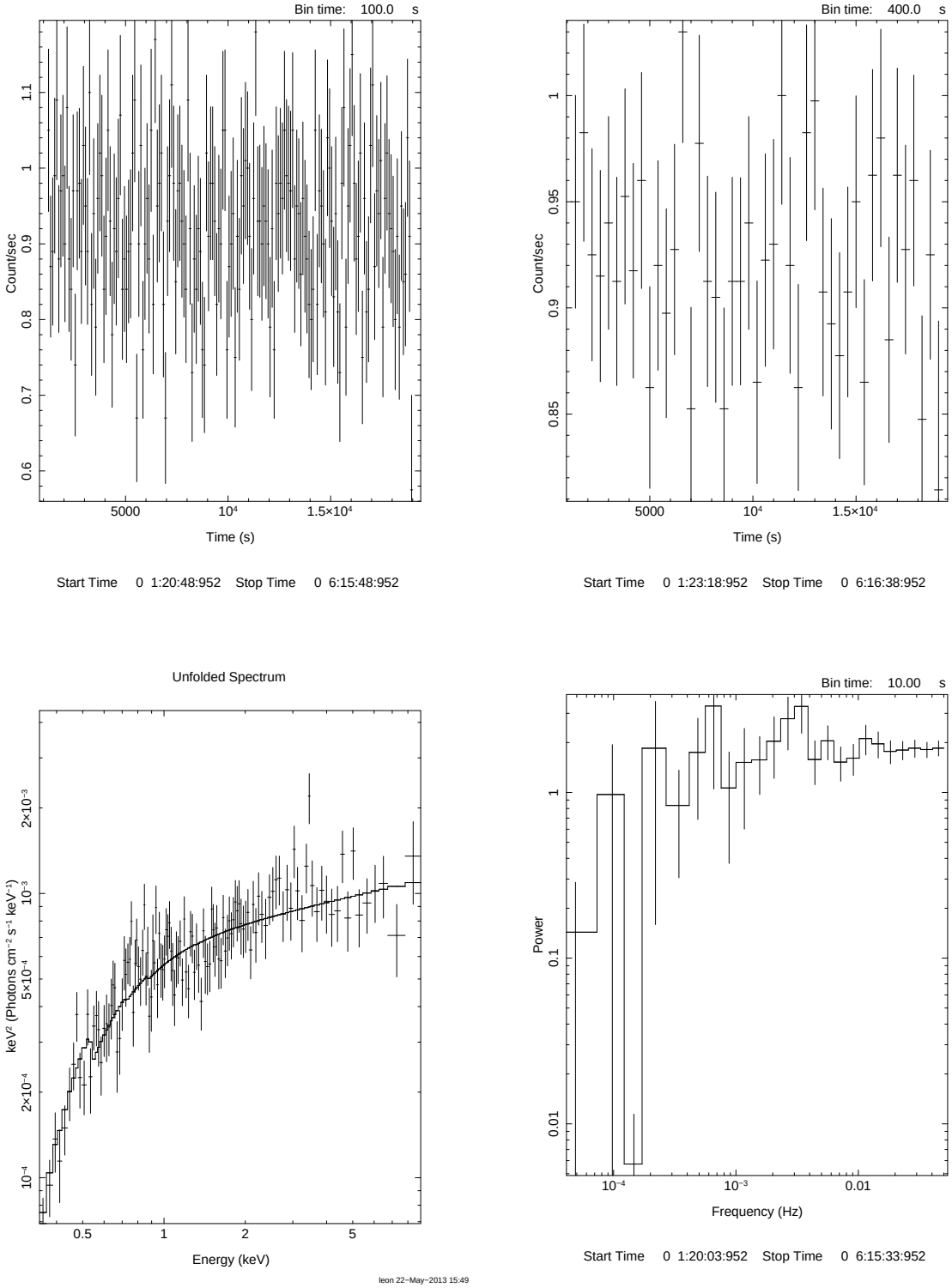

Figure 10: src10: po

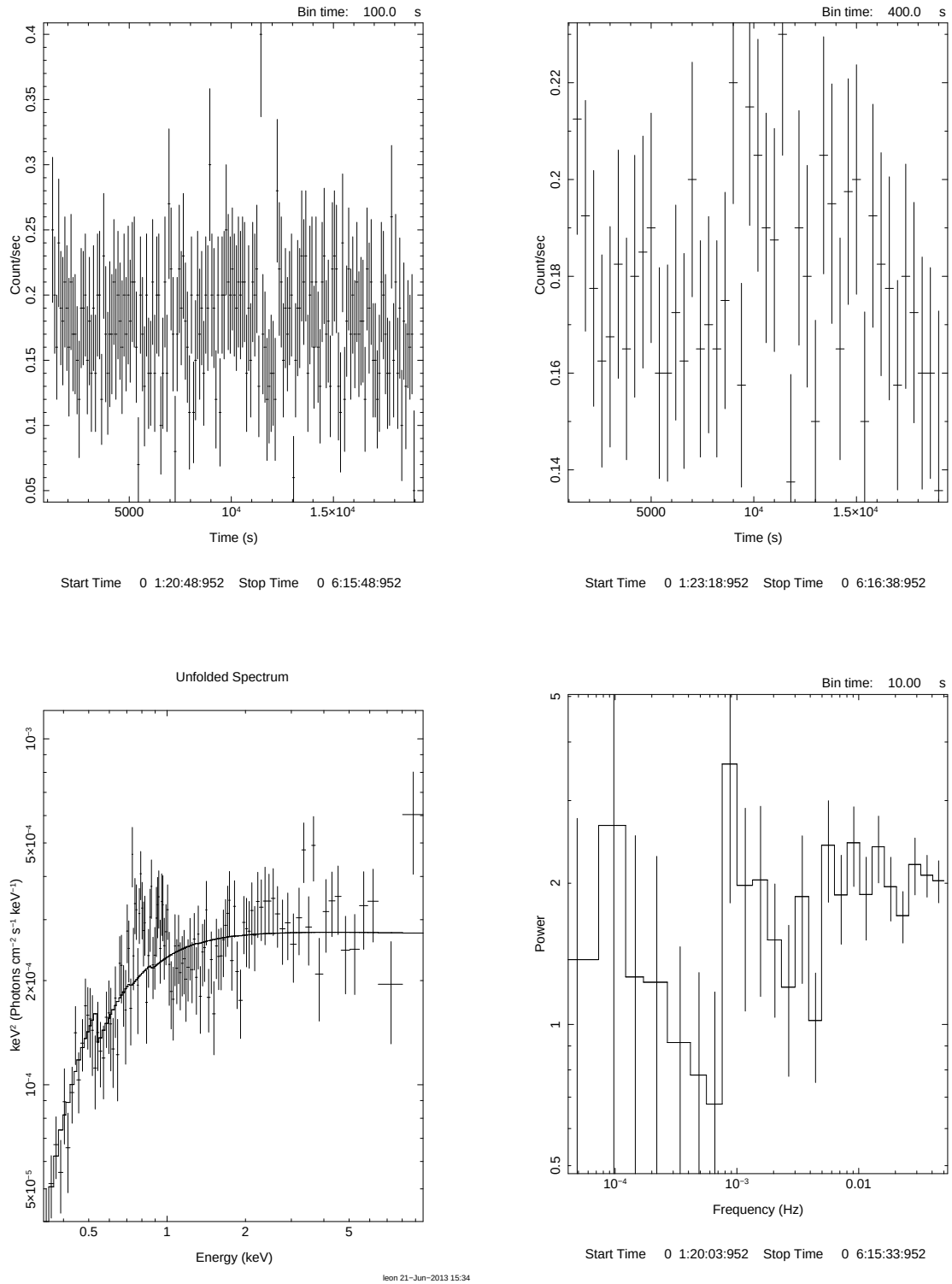

Figure 11: src11: diskbb+comptt

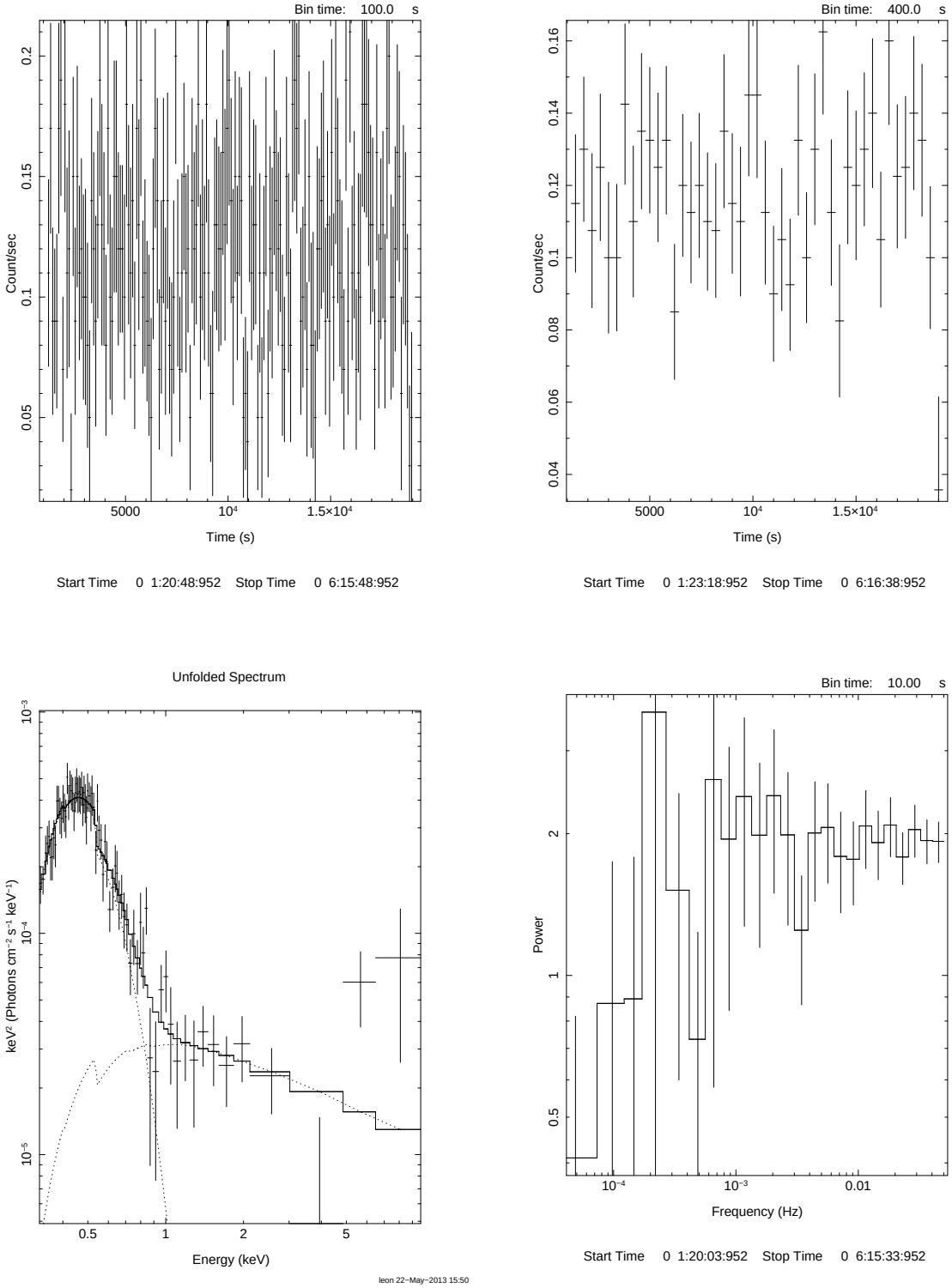

Figure 12: src12: diskbb+po

9 Appendix C

Light curves and spectra of source 10 from 2001 up to 2012.

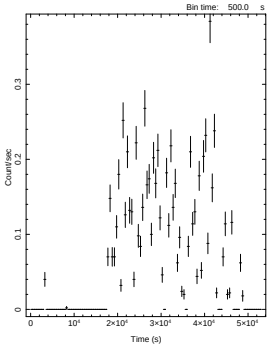

(a) 2001-06-29

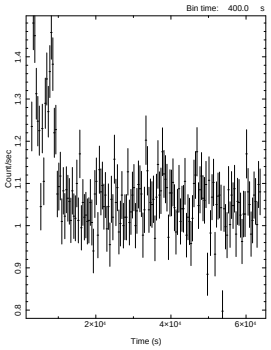

(b) 2002-01-06

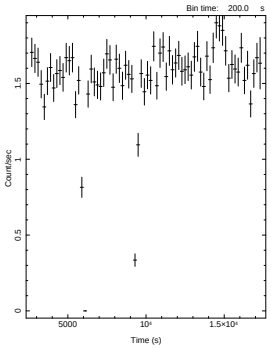

(c) 2004-07-18

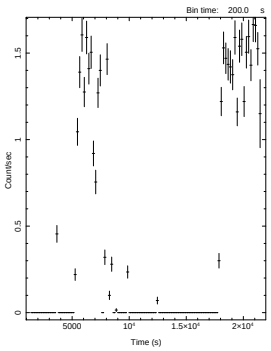

(d) 2006-08-09

Figure 1: Lightcurves 2001-2006

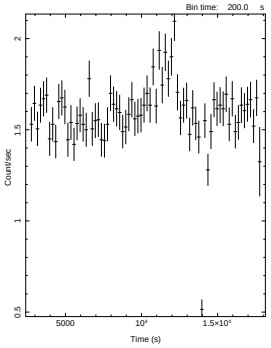

(a) 2007-02-05

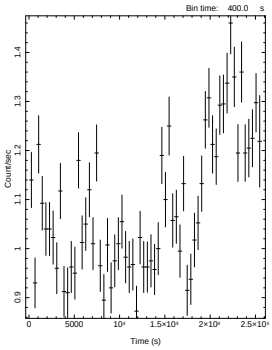

(b) 2008-01-08

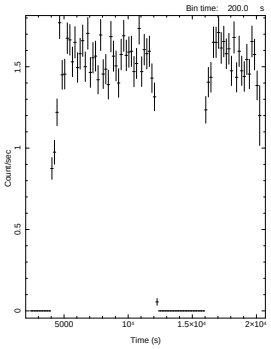

(c) 2010-01-07

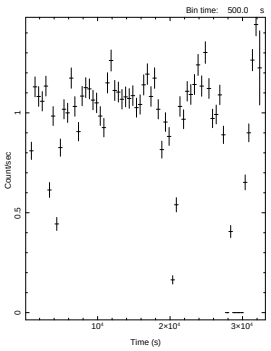

(d) 2011-01-04

Figure 2: Lightcurves 2007-2011

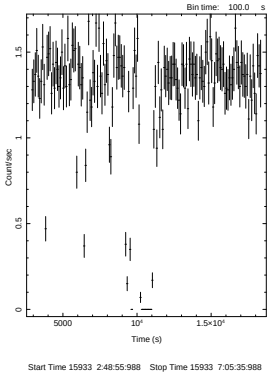

(a) 2012-01-07

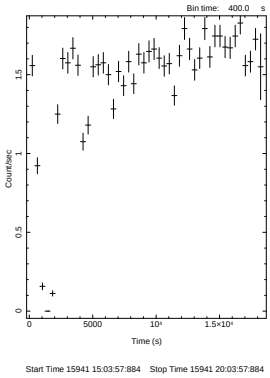

(b) 2012-01-15

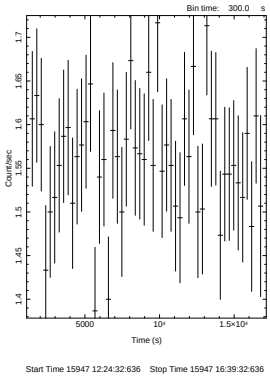

(c) 2012-01-21

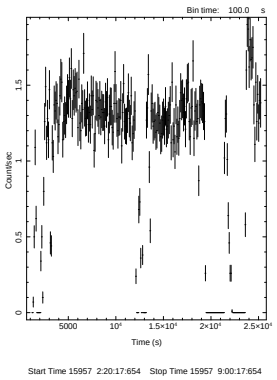

(d) 2012-01-31

Figure 3: Lightcurves 2011-2012

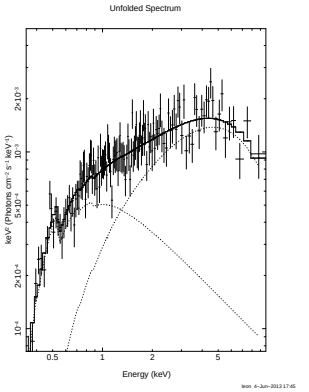

Parameter	Value
n_H	0.21(8)E22
kT_{in}	1.9(2)
$norm_{disk}$	1.4(6)E-02
Γ	2.96(67)
N_0	7.2(11)E-04
χ^2/DOF	1.0

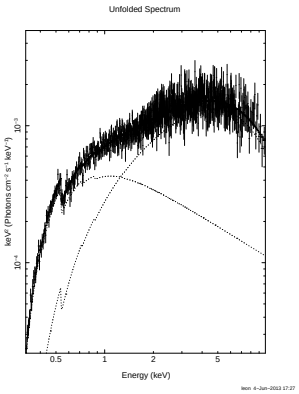

(c) 2002-01-06

Parameter	Value
n_H	0.19(2)E22
kT_{in}	1.98(4)
$norm_{disk}$	1.3(1)E-02
Γ	2.73(19)
N_0	6.0(3)E-04
χ^2/DOF	1.0

(d)

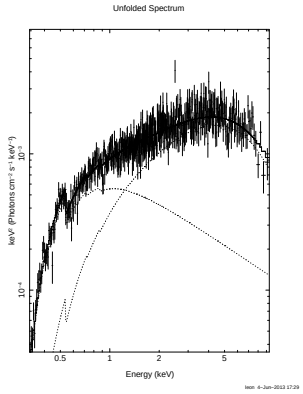

(e) 2004-07-18

Parameter	Value
n_H	0.20(3)E22
kT_{in}	1.85(5)
$norm_{disk}$	2.1(3)E-02
Γ	2.81(28)
N_0	7.8(5)E-04
χ^2/DOF	1.1

(f)

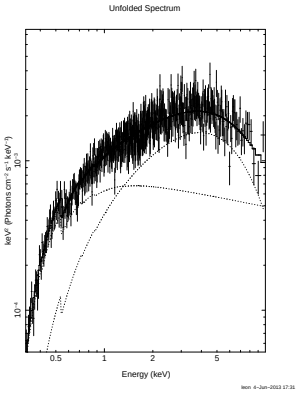

(i) 2007-02-05

Parameter	Value
n_H	0.15(2) E22
kT_{in}	1.64(8)
$norm_{disk}$	3.2(4)E-02
Γ	2.22(21)
N_0	8.1(6)E-04
χ^2/DOF	0.9

(j)

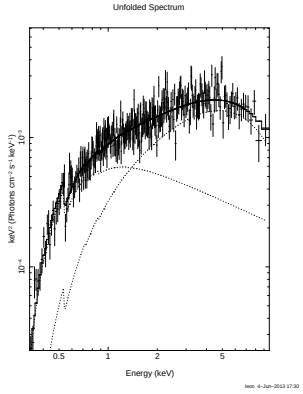

(g) 2006-08-09

Parameter	Value
n_H	0.22(5)E22
kT_{in}	2.0(1)
$norm_{disk}$	1.5(4)E-02
Γ	2.58(49)
N_0	8.3(9)
χ^2/DOF	1.1

(h)

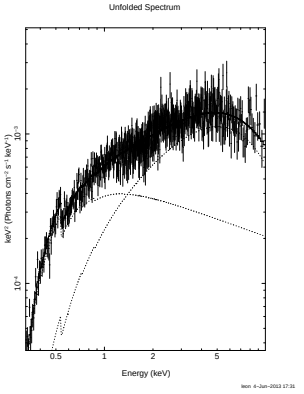

(k) 2008-01-08

Parameter	Value
n_H	0.16(2)E22
kT_{in}	2.13(6)
$norm_{disk}$	8.1(13)E-03
Γ	2.39(24)
N_0	5.0(3)E-04
χ^2/DOF	1.1

(l)

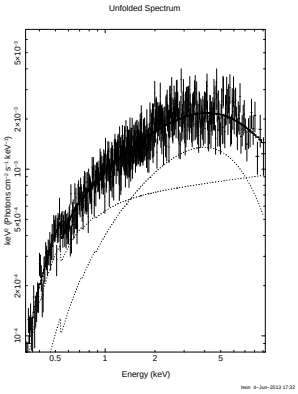

(m) 2010-01-07

Parameter	Value
n_H	0.11(2)E22
kT_{in}	1.7(2)
$norm_{disk}$	2.6(7)E-02
Γ	1.87(17)
N_0	6.8(7)E-04
χ^2/DOF	0.9

(n)

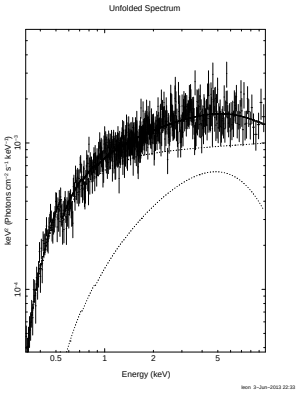

(q) 2012-01-07

Parameter	Value
n_H	0.15(2)E22
kT_{in}	2.0(3)
$norm_{disk}$	5.5(20)E-03
Γ	1.93(15)
N_0	8.4(5)E-04
χ^2/DOF	1.0

(r)

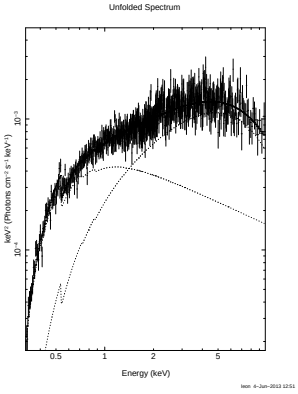

(o) 2011-01-04

Parameter	Value
n_H	0.19(2)E22
kT_{in}	2.02(6)
$norm_{disk}$	1.0(2)E-02
Γ	2.57(23)
N_0	5.8(3)E-04
χ^2/DOF	1.0

(p)

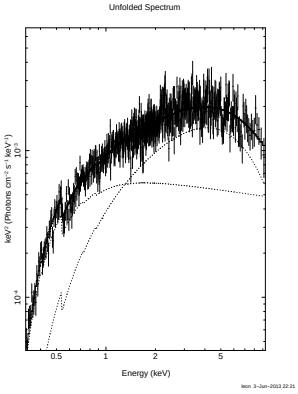

(s) 2012-01-15

Parameter	Value
n_H	0.15(2)E22
kT_{in}	1.72(8)
$norm_{disk}$	2.4(3)E-02
Γ	2.16(21)
N_0	7.0(5)E-04
χ^2/DOF	1.0

(t)

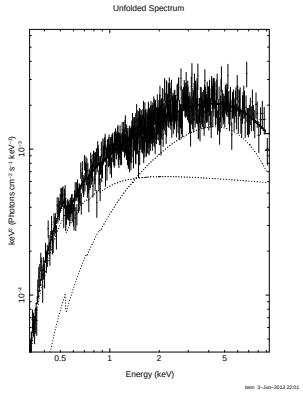

(u) 2012-01-21

Parameter	Value
n_H	0.15(2)E22
kT_{in}	1.8(1)
$norm_{disk}$	1.9(3)E-02
Γ	2.09(21)
N_0	7.2(5)E-04
χ^2/DOF	1.1

(v)

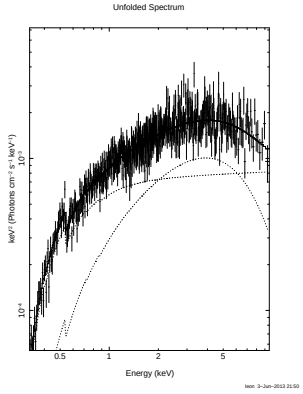

(w) 2012-01-31

Parameter	Value
n_H	0.13(2)E22
kT_{in}	1.6(1)
$norm_{disk}$	2.1(5)E-02
Γ	1.95(14) $\pm$
N_0	7.3(5)E-04
χ^2/DOF	1.0

(x)